Sivers effect in inelastic J/ψ photoproduction in $ep^{\uparrow}$ collision in color octet model

Sangem Rajesh, Raj Kishore, and Asmita Mukherjee
Department of Physics, Indian Institute of Technology Bombay, Mumbai-400076, India

(Received 7 March 2018; published 5 July 2018)

The prediction of single-spin asymmetry in inelastic photoproduction of J/ψ in $ep^{\uparrow}$ collision is presented. At next-to-leading order, the dominating process is photon-gluon fusion, $\gamma + g \to J/\psi + g$ for the production of J/ψ in $e + p^{\uparrow} \to J/\psi + X$, which directly probes the gluon Sivers function. Using the nonrelativistic QCD based color octet model, the color octet states ${}^3S_1^{(8)}$, ${}^1S_0^{(8)}$ and ${}^3P_{J(0,1,2)}^{(8)}$ contribution to J/ψ production is calculated. Sizable asymmetry is estimated as a function of transverse momentum P_T and energy fraction z of J/ψ in the range $0 < P_T \leq 1$ GeV and $0.3 < z \leq 0.9$. The unpolarized differential cross section of inelastic J/ψ photoproduction is found to be in good agreement with H1 and ZEUS data.

DOI: 10.1103/PhysRevD.98.014007

I. INTRODUCTION

Among the transverse momentum dependent pdfs (TMDs), Sivers function has attracted considerable interest in the scientific community in recent days, largely because of a large amount of experimental results coming in. The Sivers function gives the asymmetric distribution of unpolarized quarks/gluons inside a transversely polarized nucleon. The nonzero Sivers function gives a coupling between the intrinsic transverse momentum of the parton (quark/gluon) and the transverse spin of the nucleon [1,2], this gives an azimuthal asymmetry in the distribution of the final state particle in $ep^{\uparrow}$ and $pp^{\uparrow}$ collision that has been measured at HERMES [3–5], COMPASS [6–9], JLAB [10,11] and RHIC [12,13] respectively. Sivers function is a time reversal odd (T-odd) object [14]. The initial and final state interactions (gauge links) play an important role in the Sivers asymmetry. This gives a dependence on the specific process in which the Sivers function is studied. For example, Sivers function probed in semi-inclusive deep inelastic scattering (SIDIS) is expected to be the same in magnitude but opposite in sign compared to the one probed in the Drell-Yan (DY) process. More complex processes have complex gauge links [15]. Experimental data on the Sivers asymmetry have now made it possible for the extraction of u and d quark Sivers function [16], but the gluon Sivers function (GSF) is still unknown. There is no constraint on GSF except a positivity bound [17]. The GSF contains two gauge links, and the process dependence is more involved. It has been shown [18] that the GSF in any process can be written in terms of two independent Sivers functions, an f-type GSF (this contains $[++]$ gauge link and also called WW gluon distributions) and a d-type GSF (this contains $[+-]$ gauge link and are called dipole distributions) [18]. The operator structures in these two Sivers function have different charge conjugation properties.

Heavy quarkonium production in ep [19–23] and pp [24,25] collision has been studied theoretically quite extensively for probing the gluon TMDs, in particular the GSF and linearly polarized gluon distribution [26,27]. This is because the heavy quarkonium is produced at leading order (LO) through photon-gluon fusion (ep) or two gluon fusion (pp) channel. Although the production mechanism of heavy quarkonium is still not well established, the most widely used theoretical approach is based on nonrelativistic QCD (NRQCD) [28]. This gives systematic way to separate the high energy and low energy effects of the production mechanism. In this approach, the heavy quark pair is produced at a short distance in color singlet (CS) [29–32] or in color octet (CO) [33–35] configuration and then they hadronize to form a quarkonium state of given quantum numbers through a soft process. The short distance coefficients are calculated perturbatively for each process and the long distance matrix elements (LDMEs) are extracted from the experimental data. The LDMEs are categorized by performing an expansion in terms of the relative velocity of the heavy quark v in the limit $v \ll 1$ [36]. The theoretical predictions are arranged as double expansions in terms of v as well as α_s. The heavy quark pair may be produced in CO

state which then form the CS quarkonium by emitting a soft gluon. NRQCD has been successful to explain the J/ψ hadroproduction at Tevatron [37,38], also data from J/ψ photoproducton at HERA [39–42] suggests substantial contribution from CO states [43–48]. In the single-spin asymmetry (SSA) in ep collision, when the J/ψ is produced in the CS state, the two final state interactions with quark and antiquark lines cancel each other, and the final state interaction with unobserved particles cancel between diagrams having different cuts. As a result, SSA in J/ψ production in ep collision is zero when the heavy quark pair is produced in the CS state, and nonzero asymmetry can be observed when the pair is produced in CO state [49]. The final state interactions are more involved for pp collision processes, and there, nonzero SSA is expected when the heavy quark pair is produced in a CS state. In the study of TMDs in SSA in heavy quarkonium production, one assumes that TMD factorization holds for such processes.

In our previous work [20], we calculated the Sivers asymmetry in J/ψ electroproduction at LO, which is a photon-gluon $2 \to 1$ process, in color octet model (COM). We showed that the calculated asymmetry at $z = 1$ agrees within the error bar of the recent COMPASS [50] measurement. Here we extend the analysis to estimate the SSA in photoproduction of J/ψ at next-to-leading order (NLO). This allows to calculate the asymmetry over a wider kinematical region accessible to the present experiments at COMPASS and at the planned EIC in the future. We will use NRQCD based COM in our calculation for estimating the asymmetry.

The paper is organized into five sections including the introduction in Sec. I. The SSA and J/ψ production framework are presented in Sec. II and Sec. III respectively. Section IV discusses about the numerical results. The conclusion of the paper is given in Sec. V. A few details of calculation are given in the Appendices.

II. SINGLE-SPIN ASYMMETRY

In general the transverse single-spin asymmetry (SSA) is defined as following

$$A_N = \frac{d\sigma^{\uparrow} - d\sigma^{\downarrow}}{d\sigma^{\uparrow} + d\sigma^{\downarrow}}, \tag{1}$$

where $d\sigma^{\uparrow}$ and $d\sigma^{\downarrow}$ are respectively the differential cross-sections measured when one of the particle is transversely polarized up ($\uparrow$) and down ($\downarrow$) with respect to the scattering plane. Here $\uparrow(\downarrow)$ direction is the proton polarization direction along the +y (-y) axis with momentum along $-$z axis and the final hadron is produced in the xz plane as shown in Fig. 1. We consider the inclusive process $e(l) + p^{\uparrow}(P) \to J/\psi(P_h) + X$. The virtual photon radiated by the initial electron scattering will interact with the

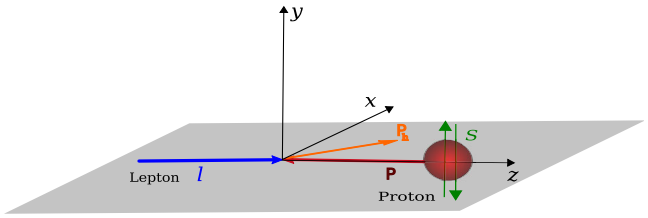

FIG. 1. Kinematical configuration for $ep \to J/\psi + X$ process.

proton. The virtual photon carries the momentum q such that $q^2 \approx -2EE'(1 - \cos\theta)$ with E and E' are energies of the initial and final electron, respectively. In the forward scattering limit, however, the four momentum of virtual photon $q^2 = -Q^2 \to 0$ as a result the virtual photon becomes the real photon. The dominating subprocess at NLO for quarkonium production in ep collision is photon-gluon fusion process, i.e., $\gamma(q) + g(k) \to J/\psi(P_h) + g(p_g)$. The letters within the round brackets represent the four momentum of each particle. There are two types of J/ψ photoproductions. One is the direct photoproduction in which the photon electromagnetically interacts with the partons of the proton. The second, resolved photoproduction wherein the photon acts as a source of partons and then they strongly interact with partons of the proton.

In this paper we have not considered the resolved photoproduction channel which basically contributes at low z region ($z \leq 0.3$) [51], where $z = \frac{P.P_h}{P.q}$ is the energy fraction transferred from the photon to J/ψ in the proton rest frame. In photoproduction, the inelastic variable z can be measured in experiments using the Jacquet-Blondel method [39,40,42]. The LO photon-gluon fusion subprocess ($\gamma + g \to J/\psi$) contributes to elastic photoproduction at $z = 1$ [20]. The process of a colorless exchanged particle between quasireal photon and proton, diffractive process, contributes to J/ψ production in the elastic region, i.e., $z \approx 1$ and $P_T \approx 0$ GeV [52,53]. P_T is the transverse momentum of J/ψ. Moreover, gluon and heavy quark fragmentation also contribute for quarkonium production significantly at $P_T > 4$ GeV [54], which are excluded by imposing P_T cut. The feed-down contribution from an excited state $\psi(2S)$ and the decay of χ_c states contribution to J/ψ are 15% [41] and 1% [53,55] respectively, are not considered in this work. Therefore, we impose the following kinematical cut $0.3 < z \leq 0.9$ to account for inelastic photoproduction [55,56] events only. For true inelastic J/ψ production, one has to impose low P_T cut as in [55,56], however, to validate asymmetry calculation in the TMD framework, we have considered $0 < P_T \leq 1$ GeV and low P_T cut is not imposed. The softening of final gluon, i.e., $z \to 1$, leads to infrared singularity in the inelastic photoproduction as shown in Eq. (B10). Hence, $z \leq 0.9$ kinematical cut is motivated to keep the final gluon hard and the perturbative calculation is under good control. At the same order in α_s, another channel $\gamma + q \to J/\psi + q$ also gives the CO contribution to J/ψ

production. Since the process is initiated by light quarks, the contribution is expected to be negligible compared to the photon-gluon fusion process [57]. For the dominating channel of J/ψ production through γg fusion, the contribution to the numerator of A_N comes mainly from the gluon Sivers distribution [58]. As the heavy quark pair in the final state is produced unpolarized, there is no contribution from Collins function [24]. Also the linearly polarized gluons do not contribute to the denominator as long as the lepton is unpolarized [58]. Within the generalized parton model formalism, the differential cross section for an unpolarized process is given by

$$E_h\frac{d\sigma}{d^3\boldsymbol{P}_h}=\frac{1}{2(2\pi)^2}\int dx_\gamma dx_g d^2\boldsymbol{k}_{\perp g} f_{\gamma/e}(x_\gamma) f_{g/p}(x_g,\boldsymbol{k}_{\perp g}) \times\delta(\hat{s}+\hat{t}+\hat{u}-M^2)\frac{1}{2\hat{s}}|\mathcal{M}_{\gamma+g\to J/\psi+g}|^2. \quad (2)$$

Here x_γ and x_g are the light-cone momentum fractions of photon and gluon respectively. The Weizsäker-Williams distribution function, $f_{\gamma/e}(x_\gamma)$, describes the density of photons inside the electron which is given by [59]

$$f_{\gamma/e}(x_\gamma)=\frac{\alpha}{2\pi}\left[2m_e^2x_\gamma\left(\frac{1}{Q^2_{\min}}-\frac{1}{Q^2_{\max}}\right)+\frac{1+(1-x_\gamma)^2}{x_\gamma}\ln\frac{Q^2_{\max}}{Q^2_{\min}}\right] \quad (3)$$

where α is the electromagnetic coupling and $Q^2_{\min}=m_e^2\frac{x_\gamma^2}{1-x_\gamma}$, m_e being the electron mass. We have considered $Q^2_{\max}=1\ \mathrm{GeV}^2$ for estimating the SSA. For photoproduction of J/ψ at HERA, we have taken two different values of $Q^2_{\max}=2.5\ \mathrm{GeV}^2$ and $1\ \mathrm{GeV}^2$ in line with H1 [39,40] and ZEUS [41,42] data, respectively. The unpolarized gluon TMD, $f_{g/p}$, represents the density of gluons inside an unpolarized proton. The $\hat{s}$, $\hat{t}$, and $\hat{u}$ are the Mandelstam variables whose definitions are given in Appendix B. $\mathcal{M}_{\gamma+g\to J/\psi+g}$ is the amplitude of photon-gluon fusion process which will be discussed in Sec. III and its square is given in Appendix A. The mass of J/ψ is represented with M. Now, we are in a position to write down the expression of numerator and denominator terms of Eq. (1) when the target proton is polarized and are given by

$$d\sigma^\uparrow-d\sigma^\downarrow=\frac{d\sigma^{ep^\uparrow\to J/\psi X}}{dzd^2\boldsymbol{P}_T}-\frac{d\sigma^{ep^\downarrow\to J/\psi X}}{dzd^2\boldsymbol{P}_T} =\frac{1}{2z(2\pi)^2}\int dx_\gamma dx_g d^2\boldsymbol{k}_{\perp g} f_{\gamma/e}(x_\gamma)\Delta^N f_{g/p^\uparrow}(x_g,\boldsymbol{k}_{\perp g})\delta(\hat{s}+\hat{t}+\hat{u}-M^2)\frac{1}{2\hat{s}}|\mathcal{M}_{\gamma+g\to J/\psi+g}|^2, \quad (4)$$

and

$$d\sigma^\uparrow+d\sigma^\downarrow=\frac{d\sigma^{ep^\uparrow\to J/\psi X}}{dzd^2\boldsymbol{P}_T}+\frac{d\sigma^{ep^\downarrow\to J/\psi X}}{dzd^2\boldsymbol{P}_T}=2\frac{d\sigma}{dzd^2\boldsymbol{P}_T} =\frac{2}{2z(2\pi)^2}\int dx_\gamma dx_g d^2\boldsymbol{k}_{\perp g} f_{\gamma/e}(x_\gamma) f_{g/p}(x_g,\boldsymbol{k}_{\perp g})\delta(\hat{s}+\hat{t}+\hat{u}-M^2)\frac{1}{2\hat{s}}|\mathcal{M}_{\gamma+g\to J/\psi+g}|^2. \quad (5)$$

The $\Delta^N f_{g/p^\uparrow}(x_g,\boldsymbol{k}_{\perp g})$, GSF, describes the density of unpolarized gluons inside the transversely polarized proton and is defined as below

$$\Delta^N f_{g/p^\uparrow}(x_g,\boldsymbol{k}_{\perp g})=f_{g/p^\uparrow}(x_g,\boldsymbol{k}_{\perp g})-f_{g/p^\downarrow}(x_g,\boldsymbol{k}_{\perp g}) =\Delta^N f_{g/p^\uparrow}(x_g,k_{\perp g})\hat{\boldsymbol{S}}.(\hat{\boldsymbol{P}}\times\hat{\boldsymbol{k}}_{\perp g}) \quad (6)$$

For estimating the SSA numerically, we have to discuss about the parametrization of TMDs. Generally, it is assumed that the unpolarized gluon TMDs follow the Gaussian distribution. The Gaussian parametrization of unpolarized TMD is

$$f_{g/p}(x_g,\boldsymbol{k}^2_{\perp g},\mu)=f_{g/p}(x_g,\mu)\frac{1}{\pi\langle k^2_{\perp g}\rangle}e^{-\boldsymbol{k}^2_{\perp g}/\langle k^2_{\perp g}\rangle}. \quad (7)$$

Here, x_g and $k_{\perp g}$ dependencies of the TMD are factorized. The collinear PDF is denoted with $f_{g/p}(x_g,\mu)$ which is measured at the scale $\mu=\sqrt{M^2+P_T^2}$. The collinear PDF obeys the Dokshitzer-Gribov-Lipatov-Altarelli-Parisi (DGLAP) scale evolution. We choose a frame (shown in Fig. 1) as discussed in Appendix B wherein the polarized proton is moving along $-z$ axis with momentum $\boldsymbol{P}$, is transversely polarized $\hat{\boldsymbol{S}}=(\cos\phi_s,\sin\phi_s,0)$. The transverse momentum of the initial gluon is $\boldsymbol{k}_{\perp g}=k_{\perp g}(\cos\phi,\sin\phi,0)$,

$$\hat{\boldsymbol{S}}.(\hat{\boldsymbol{P}}\times\hat{\boldsymbol{k}}_{\perp g})=\sin(\phi-\phi_s). \quad (8)$$

For numerical estimation we have taken $\phi_s=\pi/2$. The parametrization of GSF is given by [16,60]

TABLE I. Best fit parameters of Sivers function.

Evolution	a	N_a	α	β	ρ	M_1^2 GeV^2	$\langle k_\perp^2\rangle$ GeV^2	Notation
DGLAP	g [60]	0.65	2.8	2.8	0.687		0.25	SIDIS1
	g [60]	0.05	0.8	1.4	0.576		0.25	SIDIS2
	u [16]	0.18	1.0	6.6		0.8	0.57	BV-a
	d [16]	−0.52	1.9	10.0		0.8	0.57	BV-b

$$\Delta^N f_{g/p^\uparrow}(x_g, k_{\perp g}, \mu) = 2\mathcal{N}_g(x_g) f_{g/p}(x_g,\mu) h(k_{\perp g}) \frac{e^{-\boldsymbol{k}_{\perp g}^2/\langle k_{\perp g}^2\rangle}}{\pi\langle k_{\perp g}^2\rangle}, \quad (9)$$

here $f_{g/p}(x_g,\mu)$ is the usual collinear gluon PDF and

$$\mathcal{N}_g(x_g) = N_g x_g^\alpha (1-x_g)^\beta \frac{(\alpha+\beta)^{(\alpha+\beta)}}{\alpha^\alpha\beta^\beta}. \quad (10)$$

The definition of $h(k_{\perp g})$ is given by

$$h(k_{\perp g}) = \sqrt{2e}\frac{k_{\perp g}}{M_1} e^{-\boldsymbol{k}_{\perp g}^2/M_1^2}. \quad (11)$$

The $k_{\perp g}$ dependent part of Sivers function can be written as

$$h(k_{\perp g})\frac{e^{-\boldsymbol{k}_{\perp g}^2/\langle k_{\perp g}^2\rangle}}{\pi\langle k_{\perp g}^2\rangle} = \frac{\sqrt{2e}}{\pi}\sqrt{\frac{1-\rho}{\rho}} k_{\perp g}\frac{e^{-\boldsymbol{k}_{\perp g}^2/\rho\langle k_{\perp g}^2\rangle}}{\langle k_{\perp g}^2\rangle^{3/2}}, \quad (12)$$

where we defined

$$\rho = \frac{M_1^2}{\langle k_{\perp g}^2\rangle + M_1^2}. \quad (13)$$

D'Alesio *et al.* [60] have extracted the GSF from pion production data at RHIC [61] first time and two sets of best fit parameters were presented which are denoted with SIDIS1 and SIDIS2. Moreover, using the latest SIDIS data Anselmino *et al.* [16] have extracted the quark and antiquark Sivers function. However, GSF has not been extracted yet from SIDIS data. Therefore, in order to estimate the asymmetry, best fit parameters of Sivers function corresponding to u and d quark will be used in the following parametrizations [62]:

$$(a)\quad \mathcal{N}_g(x_g) = (\mathcal{N}_u(x_g) + \mathcal{N}_d(x_g))/2,$$
$$(b)\quad \mathcal{N}_g(x_g) = \mathcal{N}_d(x_g). \quad (14)$$

We call the parametrization (a) and (b) as BV-a and BV-b respectively. The best fit parameters are tabulated in Table I.

The final expressions of numerator and denominator terms of Eq. (1) within DGLAP evolution approach are given by

$$d\sigma^\uparrow - d\sigma^\downarrow = \frac{1}{2z(2\pi)^2}\int dx_\gamma dx_g d^2\boldsymbol{k}_{\perp g} f_{\gamma/e}(x_\gamma) 2\mathcal{N}_g(x_g) f_{g/p}(x_g,\mu)\frac{\sqrt{2e}}{\pi}\sqrt{\frac{1-\rho}{\rho}}k_{\perp g}\frac{e^{-\boldsymbol{k}_{\perp g}^2/\rho\langle k_{\perp g}^2\rangle}}{\langle k_{\perp g}^2\rangle^{3/2}} \times \delta(\hat{s}+\hat{t}+\hat{u}-M^2)\frac{1}{2\hat{s}}|\mathcal{M}_{\gamma+g\to J/\psi+g}|^2\sin(\phi-\phi_s), \quad (15)$$

and

$$d\sigma^\uparrow + d\sigma^\downarrow = \frac{2}{2z(2\pi)^2}\int dx_\gamma dx_g d^2\boldsymbol{k}_{\perp g} f_{\gamma/e}(x_\gamma) f_{g/p}(x_g,\mu)\frac{1}{\pi\langle k_{\perp g}^2\rangle} e^{-\boldsymbol{k}_{\perp g}^2/\langle k_{\perp g}^2\rangle}\delta(\hat{s}+\hat{t}+\hat{u}-M^2)\frac{1}{2\hat{s}}|\mathcal{M}_{\gamma+g\to J/\psi+g}|^2. \quad (16)$$

III. J/ψ PRODUCTION IN COM FRAMEWORK

Let us consider the J/ψ production in $e+p\to J/\psi+X$ process. The NLO subprocess is $\gamma+g\to J/\psi+g$ and the related Feynman diagrams to this process are shown in Fig. 2. The amplitude expression for bound state production in NRQCD framework can be written as below [63,64]

$$\mathcal{M}(\gamma g\to Q\bar{Q}[^{2S+1}L_J^{(1,8)}](P_h)+g) = \sum_{L_z S_z}\int\frac{d^3\boldsymbol{k}'}{(2\pi)^3}\Psi_{LL_z}(\boldsymbol{k}')\langle LL_z;SS_z|JJ_z\rangle \mathrm{Tr}[O(q,k,P_h,k')\mathcal{P}_{SS_z}(P_h,k')], \quad (17)$$

where k' is the relative momentum of the heavy quark in the quarkonium rest frame. In Eq. (17), $O(q,k,P_h,k')$ represents the amplitude of $Q\bar{Q}$ pair without considering the external heavy quark and antiquark legs, which is given by

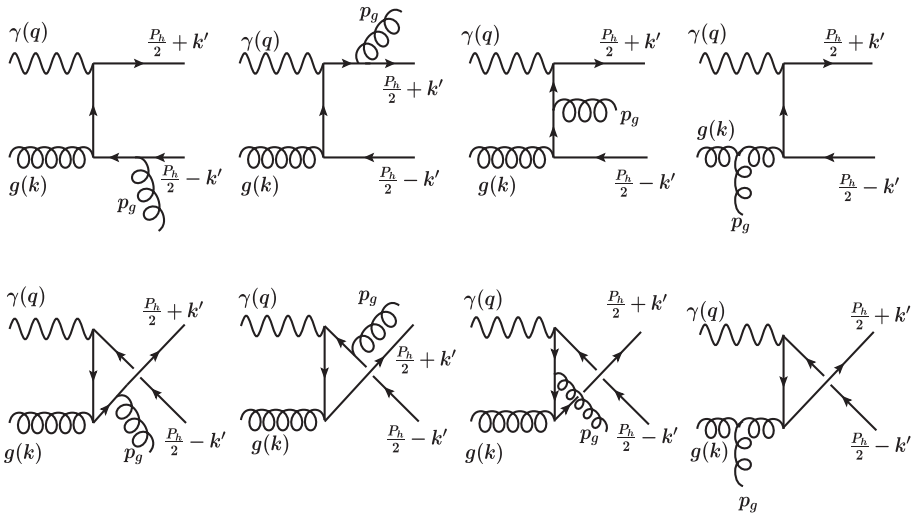

FIG. 2. Feynman diagrams for $\gamma + g \to J/\psi + g$ process.

$$O(q,k,P_h,k') = \sum_{m=1}^{8} \mathcal{C}_m O_m(q,k,P_h,k'). \tag{18}$$

From Fig. 1, the amplitude expression of individual Feynman diagram is given below

$$O_1 = 4g_s^2(ee_c)\varepsilon^{\mu}_{\lambda_a}(k)\varepsilon^{\nu}_{\lambda_b}(q)\varepsilon^{\rho *}_{\lambda_g}(p_g)\gamma_\nu \frac{\not{P}_h + 2\not{k}' - 2\not{q} + M}{(P_h + 2k' - 2q)^2 - M^2}\gamma_\mu \frac{-\not{P}_h + 2\not{k}' - 2\not{p}_g + M}{(P_h - 2k' + 2p_g)^2 - M^2}\gamma_\rho, \tag{19}$$

$$O_2 = 4g_s^2(ee_c)\varepsilon^{\mu}_{\lambda_a}(k)\varepsilon^{\nu}_{\lambda_b}(q)\varepsilon^{\rho *}_{\lambda_g}(p_g)\gamma_\rho \frac{\not{P}_h + 2\not{k}' + 2\not{p}_g + M}{(P_h + 2k' + 2p_g)^2 - M^2}\gamma_\nu \frac{-\not{P}_h + 2\not{k}' + 2\not{k} + M}{(P_h - 2k' - 2k)^2 - M^2}\gamma_\mu, \tag{20}$$

$$O_3 = 4g_s^2(ee_c)\varepsilon^{\mu}_{\lambda_a}(k)\varepsilon^{\nu}_{\lambda_b}(q)\varepsilon^{\rho *}_{\lambda_g}(p_g)\gamma_\nu \frac{\not{P}_h + 2\not{k}' - 2\not{q} + M}{(P_h + 2k' - 2q)^2 - M^2}\gamma_\rho \frac{-\not{P}_h + 2\not{k}' + 2\not{k} + M}{(P_h - 2k' - 2k)^2 - M^2}\gamma_\mu, \tag{21}$$

$$O_4 = 2g_s^2(ee_c)\varepsilon^{\mu}_{\lambda_a}(k)\varepsilon^{\nu}_{\lambda_b}(q)\varepsilon^{\rho *}_{\lambda_g}(p_g)\gamma_\nu \frac{\not{P}_h + 2\not{k}' - 2\not{q} + M}{(P_h + 2k' - 2q)^2 - M^2}\gamma^\sigma \frac{1}{(k - p_g)^2}[g_{\mu\rho}(k + p_g)_\sigma + g_{\rho\sigma}(k - 2p_g)_\mu + g_{\sigma\mu}(p_g - 2k)_\rho]. \tag{22}$$

Here $M = 2m_c$, m_c being the charm quark mass. Charge conjugation invariance implies that all the eight Feynman diagrams are symmetric by reversing the fermion flow. The amplitude expressions of O_5, O_6, O_7, and O_8 can be obtained by reversing the fermion flow and replacing $k' \to -k'$. The color factor of each diagram is given by

$$\begin{aligned}
\mathcal{C}_1 &= \mathcal{C}_6 = \mathcal{C}_7 = \sum_{ij}\langle 3i;\bar{3}j|8c\rangle(t_a t_b)_{ij},\\
\mathcal{C}_2 &= \mathcal{C}_3 = \mathcal{C}_5 = \sum_{ij}\langle 3i;\bar{3}j|8c\rangle(t_b t_a)_{ij}\\
\mathcal{C}_4 &= \mathcal{C}_8 = \sum_{ij}\langle 3i;\bar{3}j|8c\rangle i f_{abd}(t_d)_{ij}
\end{aligned} \tag{23}$$

here the summation is over the colors of the outgoing quark and antiquark. The SU(3) Clebsch-Gordan coefficients for CS and CO states, respectively, are given by

$$\langle 3i;\bar{3}j|1\rangle = \frac{\delta^{ij}}{\sqrt{N_c}}, \qquad \langle 3i;\bar{3}j|8a\rangle = \sqrt{2}(t^a)^{ij} \tag{24}$$

and they project out the color state of $Q\bar{Q}$ pair either it is in CS or CO state, where N_c is the number of colors. The generators of SU(3) group in fundamental representation is denoted by t_a which follows $\mathrm{Tr}(t_a t_b) = \delta_{ab}/2$ and $\mathrm{Tr}(t_a t_b t_c) = \frac{1}{4}(d_{abc} + i f_{abc})$. Using Eq. (24), we have the following color factors for the production of initial $Q\bar{Q}$ in CO state

$$\begin{aligned}
\mathcal{C}_1 &= \mathcal{C}_6 = \mathcal{C}_7 = \frac{\sqrt{2}}{4}(d_{abc} + i f_{abc}),\\
\mathcal{C}_2 &= \mathcal{C}_3 = \mathcal{C}_5 = \frac{\sqrt{2}}{4}(d_{abc} - i f_{abc}),\\
\mathcal{C}_4 &= \mathcal{C}_8 = \frac{\sqrt{2}}{2} i f_{abc}.
\end{aligned} \tag{25}$$

The excluded heavy quark and antiquark spinors are absorbed in the definition of spin projection operator which is given by [63,64]

$$\begin{aligned}&\mathcal{P}_{SS_z}(P_h,k')\\&=\sum_{s_1s_2}\left\langle\frac{1}{2}s_1;\frac{1}{2}s_2|SS_z\right\rangle v\left(\frac{P_h}{2}-k',s_1\right)\bar{u}\left(\frac{P_h}{2}+k',s_2\right)\\&=\frac{1}{4M^{3/2}}(-\not{P}_h+2\not{k}'+M)\Pi_{SS_z}(\not{P}_h+2\not{k}'+M)+\mathcal{O}(k'^2),\end{aligned}\tag{26}$$

bearing $\Pi_{SS_z}=\gamma^5$ for singlet ($S=0$) state and $\Pi_{SS_z}=\not{\varepsilon}_{s_z}(P_h)$ for triplet ($S=1$) state. Here spin polarization vector of the $Q\bar{Q}$ system is denoted with $\varepsilon_{s_z}(P_h)$. Since the relative momentum k' is very small with respect to P_h, Taylor expansion can be performed around $k'=0$ in Eq. (17). The first term in the expansion gives the S-wave amplitude. Since the radial wave function $R_1(0)=0$ for P-wave ($L=1, J=0, 1, 2$), one has to consider the second term in the Taylor expansion to calculate P-wave amplitude. By following Ref. [64], one obtains the S and P state amplitude expressions which are given by

$$\begin{aligned}&\mathcal{M}[^{2S+1}S_J^{(8)}](P_h,k)\\&=\frac{1}{\sqrt{4\pi}}R_0(0)\mathrm{Tr}[O(q,k,P_h,k')\mathcal{P}_{SS_z}(P_h,k')]|_{k'=0}\\&=\frac{1}{\sqrt{4\pi}}R_0(0)\mathrm{Tr}[O(0)\mathcal{P}_{SS_z}(0)],\end{aligned}\tag{27}$$

$$\begin{aligned}\mathcal{M}[^{2S+1}P_J^{(8)}]&=-i\sqrt{\frac{3}{4\pi}}R_1'(0)\sum_{L_zS_z}\varepsilon^{\alpha}_{L_z}(P_h)\langle LL_z;SS_z|JJ_z\rangle\frac{\partial}{\partial k'^{\alpha}}\mathrm{Tr}[O(q,k,P_h,k')\mathcal{P}_{SS_z}(P_h,k')]|_{k'=0}\\&=-i\sqrt{\frac{3}{4\pi}}R_1'(0)\sum_{L_zS_z}\varepsilon^{\alpha}_{L_z}(P_h)\langle LL_z;SS_z|JJ_z\rangle\mathrm{Tr}[O_{\alpha}(0)\mathcal{P}_{SS_z}(0)+O(0)\mathcal{P}_{SS_z\alpha}(0)]\end{aligned}\tag{28}$$

The following shorthand notations are defined in the above expressions

$$O(0)=O(q,k,P_h,k')|_{k'=0},\quad \mathcal{P}_{SS_z}(0)=\mathcal{P}_{SS_z}(P_h,k')|_{k'=0}\tag{29}$$

$$\begin{aligned}O_{\alpha}(0)&=\frac{\partial}{\partial k'^{\alpha}}O(q,k,P_h,k')|_{k'=0},\\\mathcal{P}_{SS_z\alpha}(0)&=\frac{\partial}{\partial k'^{\alpha}}\mathcal{P}_{SS_z}(P_h,k')|_{k'=0}.\end{aligned}\tag{30}$$

For P-wave amplitude calculation, we use the Clebsch-Gordan coefficients as defined in Refs. [65,66]

$$\sum_{L_zS_z}\langle 1L_z;SS_z|00\rangle\varepsilon^{\alpha}_{s_z}(P_h)\varepsilon^{\beta}_{L_z}(P_h)=\sqrt{\frac{1}{3}}\left(g^{\alpha\beta}-\frac{1}{M^2}P_h^{\alpha}P_h^{\beta}\right),\tag{31}$$

$$\begin{aligned}&\sum_{L_zS_z}\langle 1L_z;1S_z|1J_z\rangle\varepsilon^{\alpha}_{s_z}(P_h)\varepsilon^{\beta}_{L_z}(P_h)\\&\quad=-\frac{i}{M}\sqrt{\frac{1}{2}}\epsilon_{\delta\lambda\rho\sigma}g^{\rho\alpha}g^{\sigma\beta}P_h^{\delta}\varepsilon^{\lambda}_{J_z}(P_h),\end{aligned}\tag{32}$$

$$\sum_{L_zS_z}\langle 1L_z;1S_z|2J_z\rangle\varepsilon^{\alpha}_{s_z}(P_h)\varepsilon^{\beta}_{L_z}(P_h)=\varepsilon^{\alpha\beta}_{J_z}(P_h).\tag{33}$$

Here $\varepsilon^{\alpha}_{J_z}(P_h)$ is the polarization vector of bound state with $J=1$ and it obeys the following relations

$$\begin{aligned}\varepsilon^{\alpha}_{J_z}(P_h)P_{h\alpha}&=0,\\\sum_{L_z}\varepsilon^{\alpha}_{J_z}(P_h)\varepsilon^{*\beta}_{J_z}(P_h)&=-g^{\alpha\beta}+\frac{P_h^{\alpha}P_h^{\beta}}{M^2}\equiv\mathcal{Q}^{\alpha\beta}.\end{aligned}\tag{34}$$

The $\varepsilon^{\alpha\beta}_{J_z}(P_h)$ represents the polarization tensor for $J=2$ bound state and obeys the below relation [65,66]

$$\begin{aligned}&\varepsilon^{\alpha\beta}_{J_z}(P_h)=\varepsilon^{\beta\alpha}_{J_z}(P_h),\quad \varepsilon^{\alpha}_{J_z\alpha}(P_h)=0,\quad P_{h\alpha}\varepsilon^{\alpha}_{J_z}(P_h)=0,\\&\varepsilon^{\mu\nu}_{J_z}(P_h)\varepsilon^{*\alpha\beta}_{J_z}(P_h)=\frac{1}{2}[\mathcal{Q}^{\mu\alpha}\mathcal{Q}^{\nu\beta}+\mathcal{Q}^{\mu\beta}\mathcal{Q}^{\nu\alpha}]-\frac{1}{3}\mathcal{Q}^{\mu\nu}\mathcal{Q}^{\alpha\beta}.\end{aligned}\tag{35}$$

The $R_0(0)$ and $R_1'(0)$ are the radial wave function and its derivative at the origin, and have the following relation with LDME [57]

$$\langle 0|\mathcal{O}_1^{J/\psi}(^{2S+1}S_J)|0\rangle=\frac{N_c}{2\pi}(2J+1)|R_0(0)|^2,\tag{36}$$

$$\langle 0|\mathcal{O}_8^{J/\psi}(^{2S+1}S_J)|0\rangle=\frac{2}{\pi}(2J+1)|R_0(0)|^2,\tag{37}$$

$$\langle 0|\mathcal{O}_8^{J/\psi}(^{3}P_J)|0\rangle=\frac{2N_c}{\pi}(2J+1)|R_1'(0)|^2.\tag{38}$$

The numerical values of LDMEs are given in Table II. Now, let us discuss each CO state ($^3S_1$, $^1S_0$ ^3P_J) amplitude in detail.

TABLE II. Numerical values of LDMEs.

	$\langle\mathcal{O}_1^{J/\psi}(^3S_1)\rangle$ GeV^3	$\langle\mathcal{O}_8^{J/\psi}(^3S_1)\rangle \times 10^{-2}$ GeV^3	$\langle\mathcal{O}_8^{J/\psi}(^1S_0)\rangle \times 10^{-2}$ GeV^3	$\langle\mathcal{O}_8^{J/\psi}(^3P_0)\rangle \times 10^{-2}$ GeV^5
Ref. [45]	1.16	0.3 ± 0.12	8.9 ± 0.98	1.26 ± 0.47
Ref. [46]	1.32	0.168 ± 0.046	3.04 ± 0.35	-0.908 ± 0.161
Ref. [47]	0.645 ± 0.405	1.0 ± 0.3	0.785 ± 0.42	3.8 ± 1.1

A. $^3S_1$ amplitude

We have the following symmetry relations for $^3S_1$ state

$$\begin{aligned}
\mathrm{Tr}[O_1(0)(-\not{P}_h + M)\not{\epsilon}_{s_z}] &= \mathrm{Tr}[O_5(0)(-\not{P}_h + M)\not{\epsilon}_{s_z}] \\
\mathrm{Tr}[O_2(0)(-\not{P}_h + M)\not{\epsilon}_{s_z}] &= \mathrm{Tr}[O_6(0)(-\not{P}_h + M)\not{\epsilon}_{s_z}] \\
\mathrm{Tr}[O_3(0)(-\not{P}_h + M)\not{\epsilon}_{s_z}] &= \mathrm{Tr}[O_7(0)(-\not{P}_h + M)\not{\epsilon}_{s_z}] \\
\mathrm{Tr}[O_4(0)(-\not{P}_h + M)\not{\epsilon}_{s_z}] &= -\mathrm{Tr}[O_8(0)(-\not{P}_h + M)\not{\epsilon}_{s_z}].
\end{aligned} \tag{39}$$

Using Eq. (39), we can sum the color factors and we have

$$\mathcal{C}_1 + \mathcal{C}_5 = \mathcal{C}_2 + \mathcal{C}_6 = \mathcal{C}_3 + \mathcal{C}_7 = \frac{\sqrt{2}}{2} d_{abc} \tag{40}$$

The diagrams 4 and 8 do not contribute to $^3S_1$ state as from Eq. (39). The final amplitude expression for $^3S_1$ state can be obtained by using Eq. (27) and is given by

$$\begin{aligned}
&\mathcal{M}[^3S_1^{(8)}](P_h, k) \\
&= \frac{1}{4\sqrt{\pi M}} R_0(0) \frac{\sqrt{2}}{2} d_{abc} \mathrm{Tr}\left[\sum_{m=1}^{3} O_m(0)(-\not{P}_h + M)\not{\epsilon}_{s_z}\right],
\end{aligned} \tag{41}$$

where

$$\begin{aligned}
\sum_{m=1}^{3} O_m(0) = g_s^2 (ee_c) \varepsilon_{\lambda_a}^{\mu}(k) \varepsilon_{\lambda_b}^{\nu}(q) \varepsilon_{\lambda_g}^{\rho *}(p_g) \Bigg[&\frac{\gamma_\nu(\not{P}_h - 2\not{q} + M)\gamma_\mu(-\not{P}_h - 2\not{p}_g + M)\gamma_\rho}{(\hat{s} - M^2)(\hat{u} - M^2)} + \frac{\gamma_\rho(\not{P}_h + 2\not{p}_g + M)\gamma_\nu(-\not{P}_h + 2\not{k} + M)\gamma_\mu}{(\hat{s} - M^2)(\hat{t} - M^2)} \\
&+ \frac{\gamma_\nu(\not{P}_h - 2\not{q} + M)\gamma_\rho(-\not{P}_h + 2\not{k} + M)\gamma_\mu}{(\hat{t} - M^2)(\hat{u} - M^2)} \Bigg].
\end{aligned} \tag{42}$$

B. $^1S_0$ amplitude

The symmetry relations for $^1S_0$ state are given by

$$\begin{aligned}
\mathrm{Tr}[O_1(0)(-\not{P}_h + M)\gamma^5] &= -\mathrm{Tr}[O_5(0)(-\not{P}_h + M)\gamma^5] \\
\mathrm{Tr}[O_2(0)(-\not{P}_h + M)\gamma^5] &= -\mathrm{Tr}[O_6(0)(-\not{P}_h + M)\gamma^5] \\
\mathrm{Tr}[O_3(0)(-\not{P}_h + M)\gamma^5] &= -\mathrm{Tr}[O_7(0)(-\not{P}_h + M)\gamma^5] \\
\mathrm{Tr}[O_4(0)(-\not{P}_h + M)\gamma^5] &= \mathrm{Tr}[O_8(0)(-\not{P}_h + M)\gamma^5]
\end{aligned} \tag{43}$$

One can sum the color factors using Eq. (43) and we have the below relation

$$\mathcal{C}_1 - \mathcal{C}_5 = -\mathcal{C}_2 + \mathcal{C}_6 = -\mathcal{C}_3 + \mathcal{C}_7 = \frac{\sqrt{2}}{2} i f_{abc}, \qquad \mathcal{C}_4 + \mathcal{C}_8 = \sqrt{2} i f_{abc}. \tag{44}$$

Using Eq. (27) the final amplitude expression for $^1S_0$ state is given by

$$\mathcal{M}[^1S_0^{(8)}](P_h, k) = \frac{1}{4\sqrt{\pi M}} R_0(0) \frac{\sqrt{2}}{2} i f_{abc} \mathrm{Tr}[(O_1(0) - O_2(0) - O_3(0) + 2O_4(0))(-\not{P}_h + M)\gamma^5] \tag{45}$$

where $O_1(0)$, $O_2(0)$ and $O_3(0)$ are given in Eq. (42) and

$$O_4(0) = g_s^2 (ee_c) \varepsilon_{\lambda_a}^{\mu}(k) \varepsilon_{\lambda_b}^{\nu}(q) \varepsilon_{\lambda_g}^{\rho *}(p_g) \frac{\gamma_\nu(\not{P}_h - 2\not{q} + M)\gamma^\sigma}{\hat{u}(\hat{u} - M^2)} [g_{\mu\rho}(k + p_g)_\sigma + g_{\rho\sigma}(k - 2p_g)_\mu + g_{\sigma\mu}(p_g - 2k)_\rho]. \tag{46}$$

C. ^3P_J Amplitude

The symmetry relations for P-state ($J = 0, 1, 2$) are given by

$$\begin{aligned}
\mathrm{Tr}[O_{1\alpha}(0)\mathcal{P}_{1S_z}(0) + O_1(0)\mathcal{P}_{1\alpha S_z}(0)] &= -\mathrm{Tr}[O_{5\alpha}(0)\mathcal{P}_{1S_z}(0) + O_5(0)\mathcal{P}_{1\alpha S_z}(0)] \\
\mathrm{Tr}[O_{2\alpha}(0)\mathcal{P}_{1S_z}(0) + O_2(0)\mathcal{P}_{1\alpha S_z}(0)] &= -\mathrm{Tr}[O_{6\alpha}(0)\mathcal{P}_{1S_z}(0) + O_6(0)\mathcal{P}_{1\alpha S_z}(0)] \\
\mathrm{Tr}[O_{3\alpha}(0)\mathcal{P}_{1S_z}(0) + O_3(0)\mathcal{P}_{1\alpha S_z}(0)] &= -\mathrm{Tr}[O_{7\alpha}(0)\mathcal{P}_{1S_z}(0) + O_7(0)\mathcal{P}_{1\alpha S_z}(0)] \\
\mathrm{Tr}[O_{4\alpha}(0)\mathcal{P}_{1S_z}(0) + O_4(0)\mathcal{P}_{1\alpha S_z}(0)] &= \mathrm{Tr}[O_{8\alpha}(0)\mathcal{P}_{1S_z}(0) + O_8(0)\mathcal{P}_{1\alpha S_z}(0)]. \qquad (47)
\end{aligned}$$

From above equations, we get the color factors as given in Eq. (44). Using these color factors, the Eq. (28) can be further simplified as below

$$\begin{aligned}
\mathcal{M}[^3P_J^{(8)}](P_h,k) = \frac{\sqrt{2}}{2} f_{abc}\sqrt{\frac{3}{4\pi}}R_1'(0)\sum_{L_zS_z}\varepsilon^{\alpha}_{L_z}(P_h)\langle 1L_z;1S_z|JJ_z\rangle \\
\times \mathrm{Tr}[(O_{1\alpha}(0) - O_{2\alpha}(0) - O_{3\alpha}(0) + 2O_{4\alpha}(0))\mathcal{P}_{SS_z}(0) + (O_1(0) - O_2(0) - O_3(0) + 2O_4(0))\mathcal{P}_{SS_z\alpha}(0)]. \qquad (48)
\end{aligned}$$

In order to calculate the amplitude expression for $J = 0$, 1 and 2, we have used the Clebsch-Gordan coefficients as defined in Eqs. (31)–(33). After summing and averaging over the colors and spins, the amplitude square of each state is given in Appendix A.

IV. NUMERICAL RESULTS

In this section, we discuss the numerical results of SSA and inelastic photoproduction of J/ψ in polarized and unpolarized ep collision respectively. For numerical estimation of SSA, best fit parameters of GSF from [60] and up and down quark Sivers function parameters from [16] are considered. MSTW2008 [67] is used for PDF which is probed at the scale $\mu = \sqrt{M^2 + P_T^2}$. Mass of J/ψ, M = 3.096 GeV is taken. The NLO subprocess $\gamma + g \to J/\psi + g$ is considered for J/ψ production in $ep^\uparrow \to J/\psi + X$ process. The COM is employed for calculating production rate of J/ψ. The $^3S_1^{(8)}$, $^1S_0^{(8)}$, $^3P_0^{(8)}$, $^3P_1^{(8)}$, and $^3P_2^{(8)}$ states amplitudes are calculated using the FORM package [68], and are given in Appendix A. For comparison, we have considered three sets of LDMEs from the Refs. [45–47], which are tabulated in Table II. The LDMEs for $J = 1, 2$ are obtained by using the relations $\langle \mathcal{O}_8^{J/\psi}(^3P_1)\rangle = 3\langle \mathcal{O}_8^{J/\psi}(^3P_0)\rangle$ and $\langle \mathcal{O}_8^{J/\psi}(^3P_2)\rangle = 5\langle \mathcal{O}_8^{J/\psi}(^3P_0)\rangle$. The transverse momentum of the initial gluon $k_{\perp g}$ in Eq. (2) is integrated within the limits $0 < k_{\perp g} < 3$ GeV. We have noticed that the higher values of $k_{\perp g\,\mathrm{max}}$ (upper limit of the $k_{\perp g}$ integration) do not affect the SSA and unpolarized differential cross section.

We have estimated the SSA at $\sqrt{s} = 100$, 45 GeV (EIC) and $\sqrt{s} = 17.2$ GeV (COMPASS) energies using Eq. (1) by fixing the J/ψ production plane as discussed in [69].

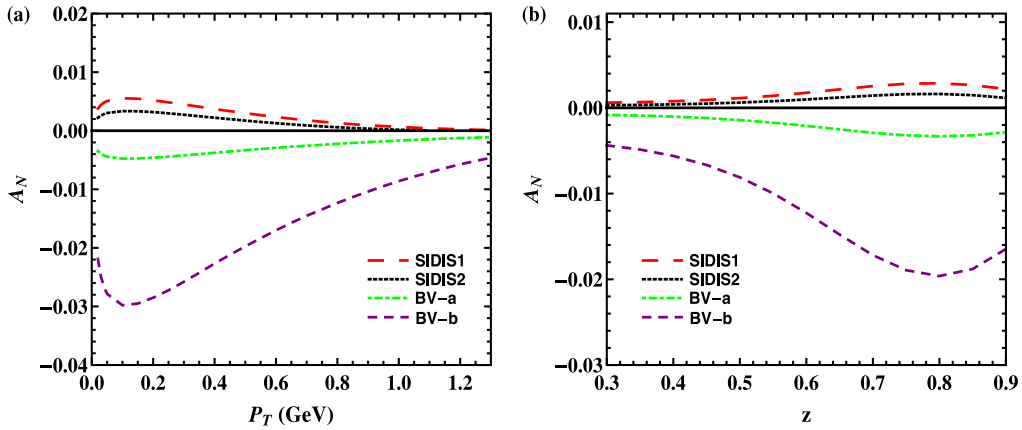

FIG. 3. Single spin asymmetry in $e + p^\uparrow \to J/\psi + X$ process as function of (a) P_T (left panel) and (b) z (right panel) at $\sqrt{s} =$ 100 GeV (EIC). The integration ranges are $0 < P_T \leq 1$ GeV and $0.3 < z < 0.9$. For convention of lines see the text.

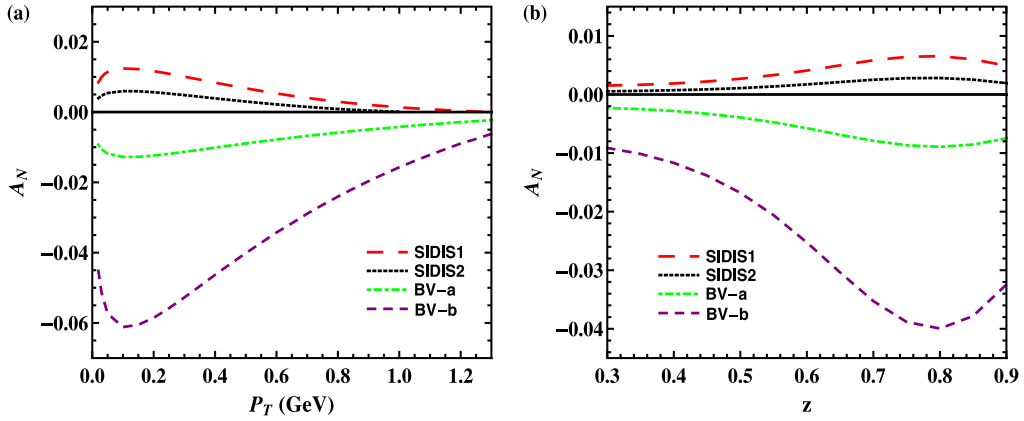

FIG. 4. Single spin asymmetry in $e + p^{\uparrow} \to J/\psi + X$ process as function of (a) P_T (left panel) and (b) z (right panel) at $\sqrt{s} = 45$ GeV (EIC). The integration ranges are $0 < P_T \leq 1$ GeV and $0.3 < z < 0.9$. For convention of lines see the text.

The SSA as a function of P_T and z is obtained by integrating $0.3 < z \leq 0.9$ and $0 < P_T \leq 1$ GeV respectively, and is shown in Figs. 3–5. The light-cone momentum fraction x_γ of quasireal photon is integrated over the range $0 < x_\gamma < 1$ in Figs. 3–6. The upper bound on the virtuality of the photon in Eq. (3), $Q^2_{\max} = 1$ GeV^2 is considered in Figs. 3–6. The integration with respect to the light-cone momentum fraction of initial gluon x_g in Eqs. (15) and (16) is carried out by using the Dirac delta function as discussed in Appendix B. The conventions in the Figs. 3–5 are the following. The obtained asymmetry using D'Alesio *et al.* [60] fit parameters of GSF is represented by "SIDIS1" and "SIDIS2." The "BV-a" and "BV-b" curves are obtained by using Anselmino *et al.* [16] fit parameters as defined in Eq. (14). As aforementioned, due to the final state interactions the asymmetry is nonzero when the heavy quark pair is produced in the CO state in ep collision [49]. Therefore, we have considered the initial heavy quark pair production is to be only in the CO state for calculating the numerator part of Eq. (1). However, the denominator of Eq. (1) is basically two times the unpolarized cross section and CS state do contribute significantly to unpolarized cross section as shown in Fig. 7. Hence, CS state contribution of J/ψ is taken into account in the denominator of asymmetry. The asymmetry is increased by maximum about 30% if the CS state contribution is not considered in the denominator. The SSA decreases as center-of-mass (C.M) energy increases in the kinematical range considered.

From Figs. 3–5, SIDIS and BV parameters are estimating positive and negative asymmetry respectively as a function of P_T and z. However, the estimated asymmetry using "SIDIS2" fit is almost close to zero for all $\sqrt{s}$. The obtained asymmetry as a function of P_T using "BV-b" parameters is maximum about 14% at COMPASS $\sqrt{s}$. Basically, asymmetry is proportional to GSF which is considered as an average of u and d quark's x-dependent normalization $\mathcal{N}(x_g)$ in "BV-a" parametrization as defined in Eq. (14). The sign of the asymmetry depends on relative magnitude of N_u and N_d and these have opposite sign which can be observed in Table I. The magnitude of $\mathcal{N}_d(x_g)$ is dominant compared to $\mathcal{N}_u(x_g)$ as a result the asymmetry is negative. The LDMEs from Ref. [45,47] estimate similar asymmetry

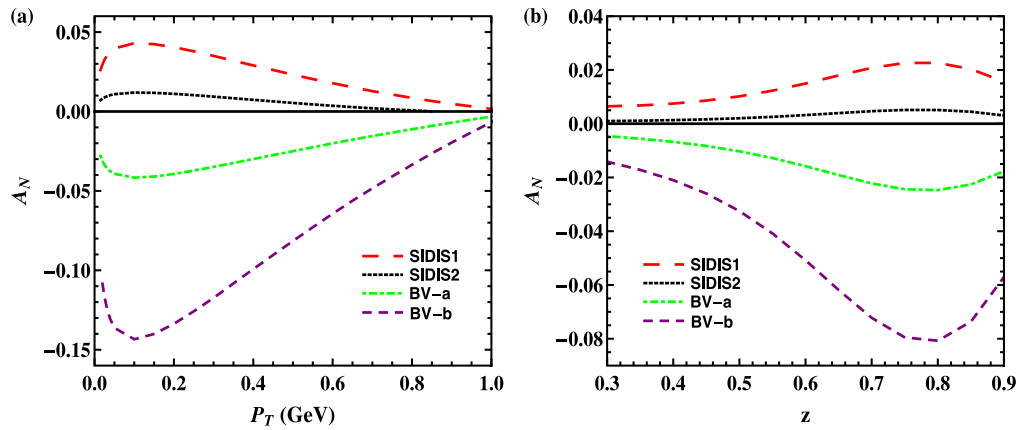

FIG. 5. Single spin asymmetry in $e + p^{\uparrow} \to J/\psi + X$ process as function of (a) P_T (left panel) and (b) z (right panel) at $\sqrt{s} = 17.2$ GeV (COMPASS). The integration ranges are $0 < P_T \leq 1$ GeV and $0.3 < z < 0.9$. For convention of lines see the text.

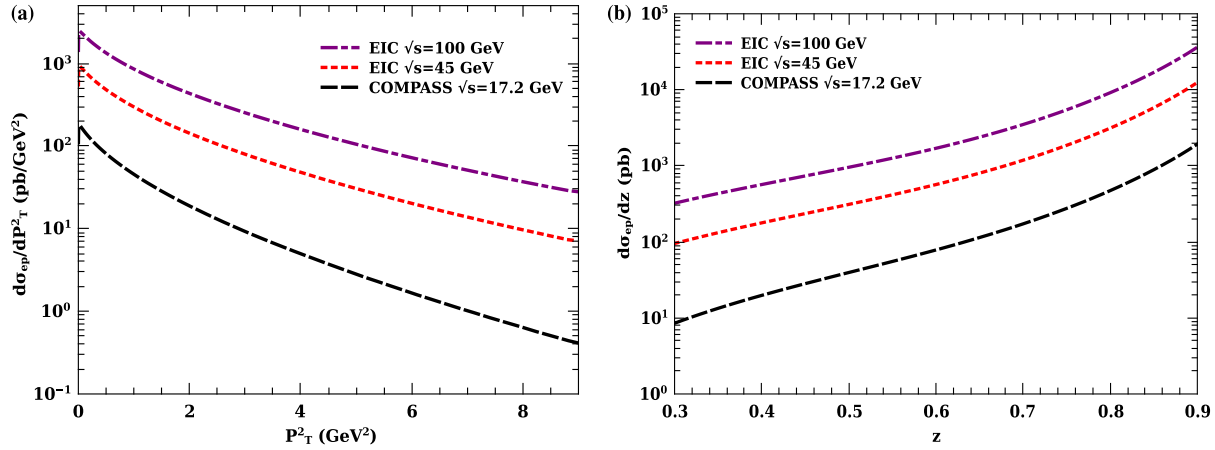

FIG. 6. Unpolarized differential cross section in $e + p \to J/\psi + X$ process as function of (a) P_T (left panel) and (b) z (right panel) at $\sqrt{s} = 100$, 45 GeV (EIC) and $\sqrt{s} = 17.2$ GeV (COMPASS) with $\langle k_{\perp g}^2 \rangle = 1$ GeV^2. The each curve is obtained by taking into account the color singlet and color octet states contribution to J/ψ production. The integration ranges are $0 < P_T \leq 3$ GeV and $0.3 < z < 0.9$. LDMEs are from [47].

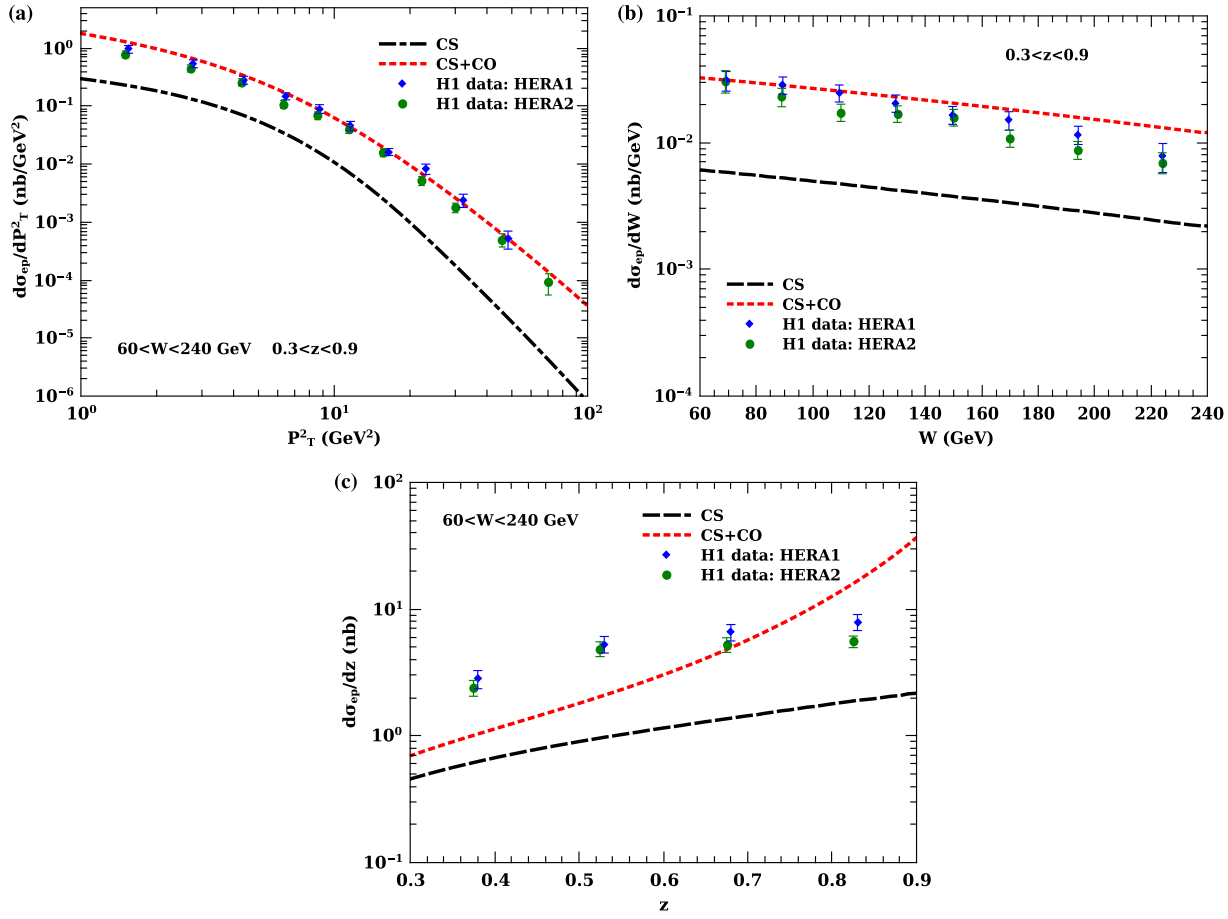

FIG. 7. Unpolarized differential cross section in $e + p \to J/\psi + X$ process as function of (a) P_T (left panel), (b) W (right panel) and (c) z (lower pannel) at HERA ($\sqrt{s} = 318$ GeV) with $\langle k_{\perp g}^2 \rangle = 1$ GeV^2. The H1 data from [39,40] and LDMEs are from [47]. The integration ranges are $1 < P_T \leq 10$ GeV, $60 < W < 240$ GeV and $0.3 < z < 0.9$. The curves "CS" and "CS + CO" represent the consideration of J/ψ production only in color singlet model and color singlet plus color octet model respectively.

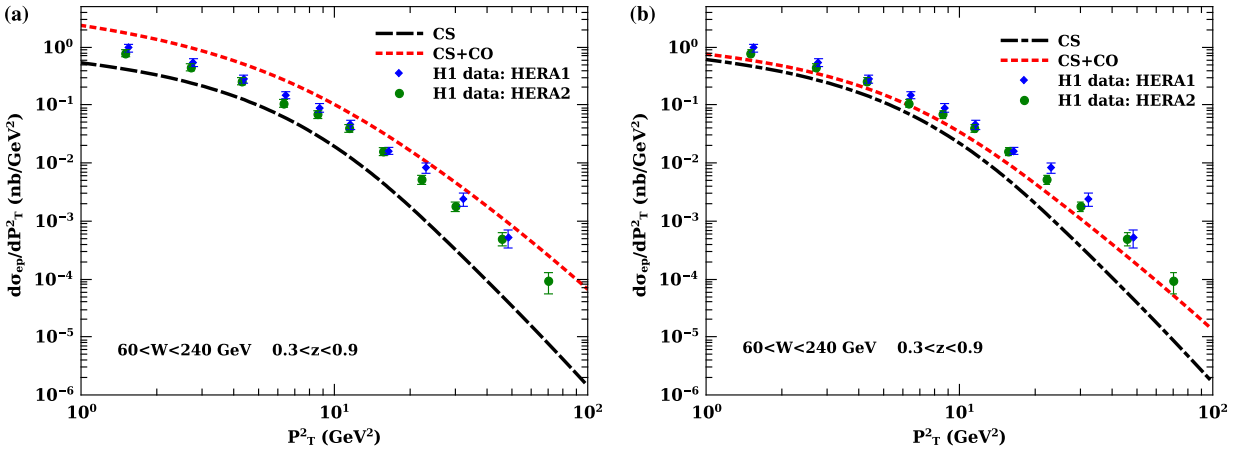

FIG. 8. Unpolarized differential cross section in $e + p \to J/\psi + X$ process as function of P_T at HERA ($\sqrt{s} = 318$ GeV) using the LDMEs from (a) Ref. [45] (left panel) and (b) Ref. [46] (right panel) with $\langle k^2_{\perp g} \rangle = 1$ GeV^2. The H1 data from [39,40]. The integration ranges are $1 < P_T \leq 10$ GeV, $60 < W < 240$ GeV and $0.3 < z < 0.9$. The convention of lines is same as Fig. 7.

as presented in Figs. 3–5. However, the obtained asymmetry using LDMEs of Ref. [46] is one order magnitude lesser than that of Figs. 3–5. This is due to the fact that CS state contribution that appear only in the denominator is much larger than CO state as shown in the right panel of Fig. 8. Nevertheless, the magnitude and sign of the asymmetry

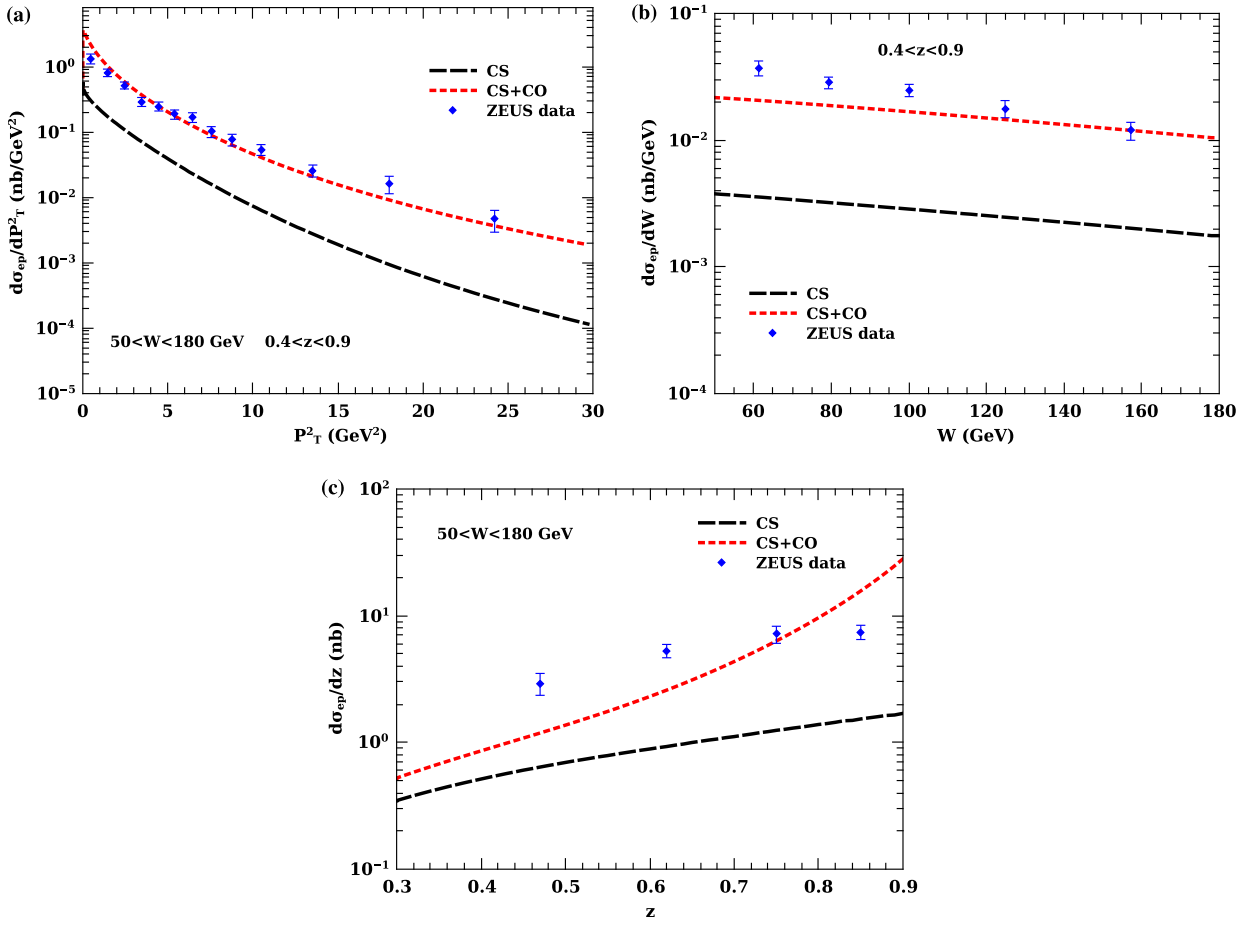

FIG. 9. Unpolarized differential cross section in $e + p \to J/\psi + X$ process as function of (a) P_T (left panel), (b) W (right panel) and (c) z (lower panel) at HERA ($\sqrt{s} = 300$ GeV) with $\langle k^2_{\perp g} \rangle = 1$ GeV^2. The ZEUS data from [41] and LDMEs are from [47]. The integration ranges are $1 < P_T \leq 5$ GeV, $50 < W < 180$ GeV and $0.4 < z < 0.9$. The convention of lines is same as Fig. 7.

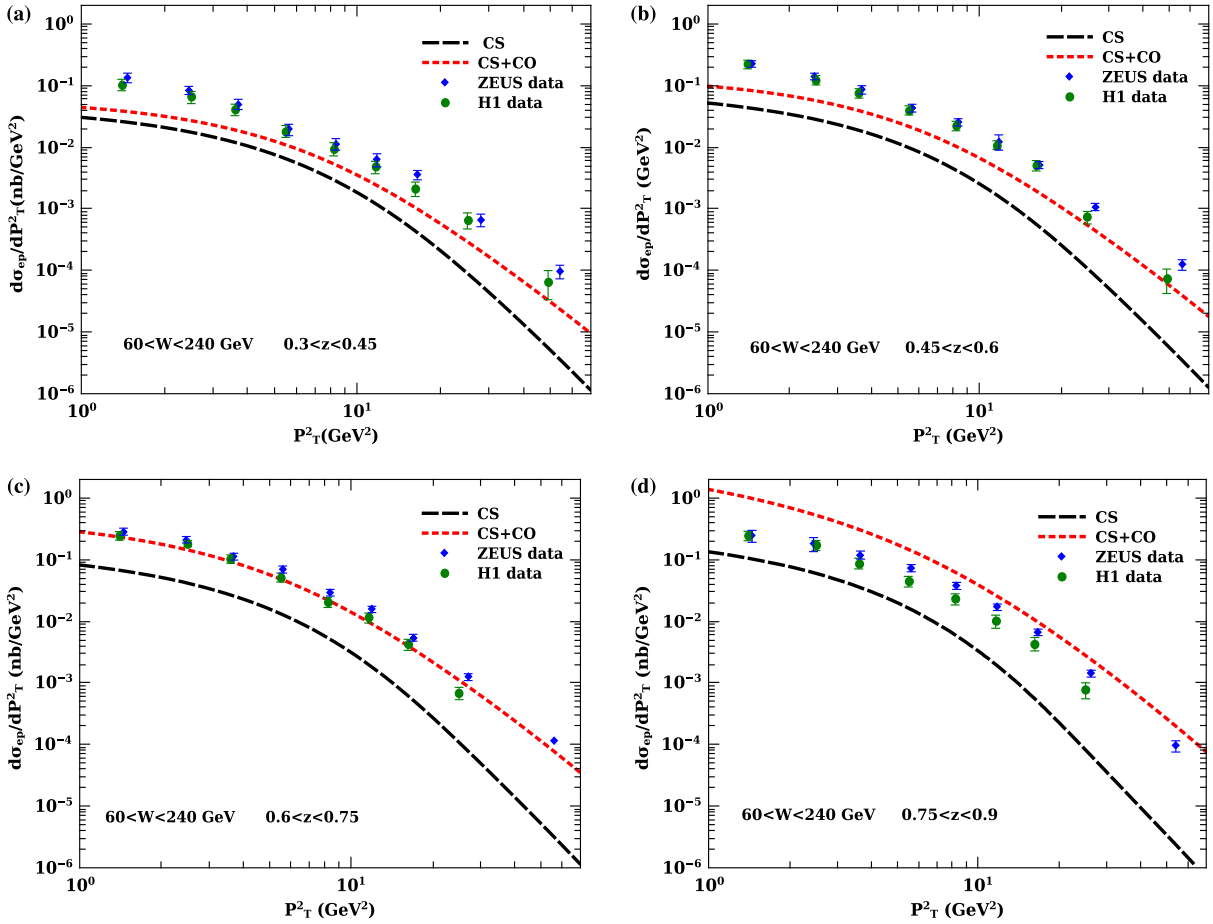

FIG. 10. Unpolarized differential cross section in $e + p \to J/\psi + X$ process as function of P_T for each z bin (a) $0.3 < z < 0.45$, (b) $0.45 < z < 0.6$, (c) $0.6 < z < 0.75$ and (d) $0.75 < z < 0.9$ at HERA ($\sqrt{s} = 318$ GeV) with $\langle k^2_{\perp g}\rangle = 1$ GeV^2. The H1, ZEUS data from [40,42] and LDMEs are from [47]. The integration range of W is $60 < W < 240$ GeV. The convention of lines is same as Fig. 7.

strongly depends on the modeling of GSF. Asymmetry increases slightly for higher values of Gaussian widths of unpolarized gluon TMD which appears in the denominator of asymmetry definition.

In Fig. 6, the unpolarized differential cross section as a function of P_T and z using the LDMEs from Ref. [47] at EIC and COMPASS energies is shown. The CS state, $^3S_1^{(1)}$, contribution to J/ψ production is considered along with CO states to obtain Fig. 6. The energy spectrum of J/ψ, right panel in Fig. 6, is restricted to $z \leq 0.9$ as we are interested in the inelastic J/ψ production. The Gaussian parametrization of gluon TMD as defined in Eq. (7) with Gaussian width $\langle k^2_{\perp g}\rangle = 1$ GeV^2 is considered. For lower values of TMD width, i.e., $\langle k^2_{\perp g}\rangle = 0.5$ GeV^2, the cross section differential in z is increased by 10% at low z region. Whereas the differential cross section as a function of P_T is increased by 4.5% in the low P_T region. The $^3P_J^{(8a)}$ state contribution to J/ψ production is significantly large compared to $^3S_1^{(8a)}$ and $^1S_0^{(8a)}$ states for the LDMEs of Ref. [47].

The obtained unpolarized differential cross section of J/ψ using the LDMEs of Ref. [47] is compared with H1 data [39,40] in Fig. 7. The theoretical results are calculated within the same kinematical region of H1 data, i.e., $\sqrt{s} = 318$ GeV, $P_T^2 > 1$ GeV^2, $60 < W < 240$ GeV, $0.3 < z < 0.9$ and $Q^2_{\max} = 2.5$ GeV^2. The C.M energy of the photon-proton system is W and $W^2 = (P + q)^2 \approx x_\gamma s$, where $s = (P + l)^2$ is the C.M energy square of the proton-lepton system. The P_T and W spectra obtained by considering the J/ψ production in CS state along with the CO states are in good agreement with data. However, the CS contribution to the J/ψ production is below the data. In Fig. 7, the $d\sigma/dz$ distribution is not well described by both CS and CO contributions of J/ψ. From Fig. 7, it is obvious that the CO states contribution is dominated for higher z values.

The H1 data are compared with the theoretical results obtained by using the LDMEs of Ref. [45,46], which are presented in Fig. 8. The LDMEs of [45] over estimate the result as shown in the left panel of Fig. 8. Whereas Ref. [46] LDMEs predict the result very close to the data,

TABLE III. χ^2/d.o.f for the LDMEs of Refs. [45–47].

Data	LDMEs of [45]	LDMEs of [46]	LDMEs of [47]
H1 data [40]	62.129	3.83	7.92
ZEUS data [41]	12.56	9.12	2.541

which is illustrated in the right panel of Fig. 8. The same behavior is also noticed for z and W spectra which are not shown. To assess the agreement between the data and theoretical results, χ^2/d.o.f is calculated for three sets of LDMEs from the P_T spectrum of Figs. 7–9 at a fixed $\langle k_{\perp g}^2\rangle = 1$ GeV^2, which is tabulated in Table III. The χ^2/d.o.f for $\langle k_{\perp g}^2\rangle = 1$ GeV^2 is observed to be smaller than that of $\langle k_{\perp g}^2\rangle = 0.5$ GeV^2 and $\langle k_{\perp g}^2\rangle = 0.25$ GeV^2 for three sets of LDMEs. Therefore, we have considered the unpolarized TMD Gaussian width to be $\langle k_{\perp g}^2\rangle = 1$ GeV^2 in the analysis of J/ψ photoproduction. Since the χ^2/d.o.f for LDMEs of [47] is 7.92 and 2.541 for H1 and ZEUS data respectively, only the LDMEs of Ref. [47] have been used in the Figs. 9 and 10. The ZEUS data [41] are compared with theoretical results within the kinematical region $\sqrt{s} = 300$ GeV, $50 < W < 180$ GeV, $0.4 < z < 0.9$, and $Q^2_{\max} = 1$ GeV^2, and is shown in Fig. 9. The W and z spectra are obtained by integrating the P_T over the range $1 < P_T < 5$ GeV. In Fig. 10, the P_T spectrum for each z bin is compared with H1 [40] and ZEUS [42] data. The P_T spectrum is away from the data in the $0.3 < z < 0.5$, $0.45 < z < 0.6$, and $0.75 < z < 0.9$ bins. However, the theoretical result is in good agreement with the data for the bin $0.6 < z < 0.75$.

V. CONCLUSION

We have calculated the single-spin asymmetry and unpolarized differential cross section in the inelastic photoproduction of J/ψ in polarized and unpolarized ep collision respectively, where the scattered electron with small angle produces low virtuality photons. The NLO subprocess for J/ψ production is the photon-gluon fusion process $\gamma + g \to J/\psi + g$. Within the NRQCD based COM framework, the color octet states ${}^3S_1^{(8)}$, ${}^1S_0^{(8)}$, and ${}^3P_{J(0,1,2)}^{(8)}$ contribution to J/ψ production is calculated. Sizable asymmetry is obtained as a function of P_T and z in the kinematical range $0 < P_T \leq 1$ GeV and $0.3 < z \leq 0.9$ respectively. The infrared singularity at $z = 1$, arises when the final gluon becomes soft, is excluded by restricting the analysis in the region $z \leq 0.9$. The resolved photoproduction contribution is removed by considering $z > 0.3$. We also presented the unpolarized differential cross section of inelastic J/ψ photoproduction as a function of P_T, z, and W, and is found to be in good agreement with the H1 and ZEUS data. The sizable asymmetry indicates that the inelastic photoproduction of J/ψ in $ep^\uparrow$ collision is a useful process to probe the gluon Sivers function over a wide kinematical region accessible to the future electron-ion collider (EIC).

ACKNOWLEDGEMENT

We would like to thank Jean-Philippe Lansberg for fruitful discussion during his stay at IIT Bombay.

APPENDIX A: SQUARE OF THE AMPLITUDE FOR $\gamma + g \to J/\psi + g$ PROCESS

The summation over only the transverse polarizations of the initial and final on-shell gluons and photon is achieved by invoking [63]

$$\sum_{\lambda_a=1}^{2} \varepsilon_\mu^{\lambda_a}(k)\varepsilon_{\mu'}^{*\lambda_a}(k) = -g_{\mu\mu'} + \frac{k_\mu n_{\mu'} + k_{\mu'} n_\mu}{k.n} - \frac{k_\mu k_{\mu'}}{(k.n)^2} \quad \text{(A1)}$$

with $n^\mu = \frac{P_h^\mu}{M}$. We define the following variables for computation purpose

$$s_1 = \hat{s} - M^2, \qquad t_1 = \hat{t} - M^2, \qquad u_1 = \hat{u} - M^2. \quad \text{(A2)}$$

FORM package [68] is used to obtain the square of the amplitude. The CS, ${}^3S_1^{(1)}$ state amplitude calculation is similar to CO, ${}^3S_1^{(8a)}$, except a change in the color factor. The amplitude square of ${}^3S_1^{(1,8)}$, ${}^1S_0^{(8)}$, ${}^3P_0^{(8)}$, ${}^3P_1^{(8)}$, and ${}^3P_2^{(8)}$ states is given below

$$|\mathcal{M}[{}^3S_1^{(1)}]|^2 = \frac{2\pi^3 e_c^2 \alpha_s^2 \alpha}{27M} \langle 0|\mathcal{O}_1^{J/\psi}({}^3S_1)|0\rangle \frac{512M^2}{s_1^2 t_1^2 u_1^2}\{s_1^2(s_1+M^2)^2 + u_1^2(u_1+M^2)^2 + t_1^2(t_1+M^2)^2\} \quad \text{(A3)}$$

$$|\mathcal{M}[{}^3S_1^{(8)}]|^2 = \frac{5\pi^3 e_c^2 \alpha_s^2 \alpha}{36M} \langle 0|\mathcal{O}_8^{J/\psi}({}^3S_1)|0\rangle \frac{512M^2}{s_1^2 t_1^2 u_1^2}\{s_1^2(s_1+M^2)^2 + u_1^2(u_1+M^2)^2 + t_1^2(t_1+M^2)^2\} \quad \text{(A4)}$$

$$|\mathcal{M}[^1S_0^{(8)}]|^2 = \frac{3\pi^3 e_c^2\alpha_s^2\alpha}{4M}\langle 0|\mathcal{O}_8^{J/\psi}(^1S_0)|0\rangle \frac{128}{s_1^2t_1^2u_1^2(M^2+u_1)^2}\{8M^{14}+4M^{12}$$
$$\times(4(s_1+t_1)+7u_1)+2M^{10}(8s_1^2+17u_1(s_1+t_1)+12s_1t_1+8t_1^2+19u_1^2)$$
$$+2M^8(7s_1^3+4u_1(s_1^2+5s_1t_1+t_1^2)+5s_1^2t_1+5s_1t_1^2+6u_1^2(s_1+t_1)+7t_1^3$$
$$+13u_1^3)+2M^6(2s_1^4+4u_1(s_1^3+t_1^3)+s_1^3t_1+u_1^2(-17s_1^2+7s_1t_1-17t_1^2)$$
$$+2s_1^2t_1^2+s_1t_1^3-8u_1^3(s_1+t_1)+2t_1^4+5u_1^4)+2M^4(6u_1^3(-3s_1^2+s_1t_1-3t_1^2)$$
$$-6u_1^2(s_1+t_1)(s_1^2+t_1^2)+u_1(s_1-t_1)^2(s_1^2+4s_1t_1+t_1^2)-6u_1^4(s_1+t_1)$$
$$-3s_1t_1(s_1-t_1)^2(s_1+t_1)+u_1^5)+M^2(-2u_1^4(5s_1^2-11s_1t_1+5t_1^2)+u_1^2$$
$$\times(-2s_1^4+s_1^3t_1-5s_1^2t_1^2+s_1t_1^3-2t_1^4)-2u_1^5(s_1+t_1)-6u_1^3(s_1-t_1)^2(s_1+t_1)$$
$$+s_1t_1u_1(s_1-t_1)^2(s_1+t_1)-s_1t_1(s_1-t_1)^2(2s_1+t_1)(s_1+2t_1))$$
$$+s_1t_1u_1(3u_1^2(s_1^2+s_1t_1+t_1^2)+(s_1-t_1)^2(s_1^2+s_1t_1+t_1^2)+8u_1^3(s_1+t_1)+8u_1^4)\} \quad \text{(A5)}$$

$$|\mathcal{M}[^3P_0^{(8)}]|^2 = \frac{\pi^3 e_c^2\alpha_s^2\alpha}{4M}\langle 0|\mathcal{O}_8^{J/\psi}(^3P_0)|0\rangle \frac{512}{M^2s_1^4t_1^4u_1^4(M^2+u_1)^2}\{32s_1t_1u_1M^{20}$$
$$+16(-5s_1^2t_1^2-(s_1^2-8t_1s_1+t_1^2)u_1^2)M^{18}+16u_1(s_1t_1(2s_1^2-13t_1s_1+2t_1^2)$$
$$-2(s_1^2-6t_1s_1+t_1^2)u_1^2)M^{16}+8(2(s_1^2+8t_1s_1+t_1^2)u_1^4+s_1t_1(2s_1^2-17t_1s_1$$
$$+2t_1^2)u_1^2-2s_1^2t_1^2(3s_1^2-7t_1s_1+3t_1^2))M^{14}+8u_1(2(5s_1^2+2t_1s_1+5t_1^2)u_1^4$$
$$-(2s_1^4+15t_1s_1^3-19t_1^2s_1^2+15t_1^3s_1+2t_1^4)u_1^2-s_1t_1(s_1^4+8t_1s_1^3-22t_1^2s_1^2$$
$$+8t_1^3s_1+t_1^4))M^{12}+4(16(s_1^2+t_1^2)u_1^6-(3s_1^2+16t_1s_1+3t_1^2)(4s_1^2-7t_1s_1$$
$$+4t_1^2)u_1^4+s_1t_1(3s_1^4+4t_1s_1^3-2t_1^2s_1^2+4t_1^3s_1+3t_1^4)u_1^2+2s_1^2t_1^2(2s_1^4$$
$$+7t_1s_1^3-10t_1^2s_1^2+7t_1^3s_1+2t_1^4))M^{10}+4u_1(4(s_1^2+t_1^2)u_1^6-(12s_1^4$$
$$+19t_1s_1^3-73t_1^2s_1^2+19t_1^3s_1+12t_1^4)u_1^4+s_1t_1(11s_1^4+6t_1s_1^3-26t_1^2s_1^2$$
$$+6t_1^3s_1+11t_1^4)u_1^2-s_1^2t_1^2(s_1+t_1)^4)M^8+2(-2(4s_1^4+t_1s_1^3-32t_1^2s_1^2$$
$$+t_1^3s_1+4t_1^4)u_1^6+s_1t_1(10s_1^4-19t_1s_1^3-15t_1^2s_1^2-19t_1^3s_1+10t_1^4)u_1^4$$
$$-s_1^2t_1^2(11s_1^4+3t_1s_1^3-22t_1^2s_1^2+3t_1^3s_1+11t_1^4)u_1^2-2s_1^3(s_1-t_1)^2t_1^3$$
$$\times(2s_1+t_1)(s_1+2t_1))M^6+2s_1t_1u_1(2(s_1^2+7t_1s_1+t_1^2)u_1^6-(2s_1^4+11t_1s_1^3$$
$$-12t_1^2s_1^2+11t_1^3s_1+2t_1^4)u_1^4+s_1t_1(s_1^4+10t_1s_1^3+10t_1^2s_1^2+10t_1^3s_1+t_1^4)u_1^2$$
$$+6s_1^2t_1^2(s_1^2-t_1^2)^2)M^4+s_1^2t_1^2u_1^2(2(4s_1^2+11t_1s_1+4t_1^2)u_1^4+(4s_1^4-16t_1s_1^3$$
$$-19t_1^2s_1^2-16t_1^3s_1+4t_1^4)u_1^2-3s_1(s_1-t_1)^2t_1(2s_1^2+3t_1s_1+2t_1^2))M^2+s_1^3t_1^3$$
$$\times(s_1^2+t_1s_1+t_1^2)u_1^3((s_1-t_1)^2+3u_1^2)\} \quad \text{(A6)}$$

$$|\mathcal{M}[^3P_1^{(8)}]|^2 = \frac{\pi^3 e_c^2\alpha_s^2\alpha}{8M}\langle 0|\mathcal{O}_8^{J/\psi}(^3P_1)|0\rangle \frac{2048}{m^2s_1^4t_1^4u_1^4(m^2+u_1)^2}\{8s_1t_1u_1m^{20}+4(5s_1^2t_1^2$$
$$+(s_1+t_1)^2u_1^2)m^{18}+4u_1(2(s_1^2-4t_1s_1+t_1^2)u_1^2+s_1t_1(5s_1^2+8t_1s_1+5t_1^2))$$
$$\times m^{16}+2(-2(s_1^2+16t_1s_1+t_1^2)u_1^4+s_1t_1(12s_1^2+23t_1s_1+12t_1^2)u_1^2+2s_1^2t_1^2$$
$$\times(3s_1^2-7t_1s_1+3t_1^2))m^{14}+2u_1(-10(s_1+t_1)^2u_1^4+(2s_1^4-16t_1s_1^3+71t_1^2s_1^2$$
$$-16t_1^3s_1+2t_1^4)u_1^2+s_1t_1(-2s_1^4+3t_1s_1^3-22t_1^2s_1^2+3t_1^3s_1-2t_1^4))m^{12}$$

$$
\begin{aligned}
&+(-(16s_1^2+7t_1s_1+16t_1^2)u_1^6+2(6s_1^4-31t_1s_1^3+109t_1^2s_1^2-31t_1^3s_1+6t_1^4)u_1^4\\
&-s_1t_1(3s_1^4+16t_1s_1^3+20t_1^2s_1^2+16t_1^3s_1+3t_1^4)u_1^2-2s_1^2t_1^2(2s_1^4+7t_1s_1^3-10t_1^2s_1^2\\
&+7t_1^3s_1+2t_1^4))m^{10}+u_1((-4s_1^2+3t_1s_1-4t_1^2)u_1^6+(12s_1^4-28t_1s_1^3+159t_1^2s_1^2\\
&-28t_1^3s_1+12t_1^4)u_1^4+s_1t_1(5s_1^4-16t_1s_1^3-45t_1^2s_1^2-16t_1^3s_1+5t_1^4)u_1^2-s_1^2t_1^2\\
&\times(3s_1^4+5t_1s_1^3-12t_1^2s_1^2+5t_1^3s_1+3t_1^4))m^8+(3s_1t_1u_1^8+(4s_1^4+55t_1^2s_1^2+4t_1^4)\\
&\times u_1^6+s_1t_1(3s_1^4-16t_1s_1^3-87t_1^2s_1^2-16t_1^3s_1+3t_1^4)u_1^4+s_1t_1(2s_1^6-t_1s_1^5+21t_1^2s_1^4\\
&-15t_1^3s_1^3+21t_1^4s_1^2-t_1^5s_1+2t_1^6)u_1^2+s_1^3(s_1-t_1)^2t_1^3(2s_1+t_1)(s_1+2t_1))m^6\\
&+s_1t_1u_1(u_1^8+(2s_1^2+3t_1s_1+2t_1^2)u_1^6-(s_1^4+12t_1s_1^3+59t_1^2s_1^2+12t_1^3s_1+t_1^4)u_1^4\\
&+(2s_1^6-7t_1s_1^5+24t_1^2s_1^4-7t_1^3s_1^3+24t_1^4s_1^2-7t_1^5s_1+2t_1^6)u_1^2-s_1^2(s_1-t_1)^2\\
&\times t_1^2(s_1^2+t_1s_1+t_1^2))m^4-s_1^2t_1^2u_1^2(3u_1^6+(2s_1^2+13t_1s_1+2t_1^2)u_1^4\\
&+(5s_1^4-13t_1s_1^3-7t_1^2s_1^2-13t_1^3s_1+5t_1^4)u_1^2+s_1^2(s_1-t_1)^2t_1^2)m^2\\
&+s_1^3t_1^3(s_1^2+t_1s_1+t_1^2)u_1^3((s_1-t_1)^2+3u_1^2)\}
\end{aligned}
\tag{A7}
$$

$$
\begin{aligned}
|\mathcal{M}[^3P_2^{(8)}]|^2=&\frac{3\pi^3e_c^2\alpha_s^2\alpha}{20M}\langle 0|\mathcal{O}_8^{J/\psi}(^3P_2)|0\rangle\frac{1024}{3M^2s_1^4t_1^4u_1^4(M^2+u_1)^2}\{104s_1t_1u_1M^{20}+4\\
&\times(-5s_1^2t_1^2-(s_1^2-86t_1s_1+t_1^2)u_1^2)M^{18}+4u_1((-2s_1^2+99t_1s_1-2t_1^2)u_1^2\\
&+2s_1t_1(13s_1^2-23t_1s_1+13t_1^2))M^{16}+2(2(s_1^2+47t_1s_1+t_1^2)u_1^4+s_1t_1\\
&\times(122s_1^2-107t_1s_1+122t_1^2)u_1^2-2s_1^2t_1^2(3s_1^2-7t_1s_1+3t_1^2))M^{14}+2u_1\\
&\times(10(s_1^2+4t_1s_1+t_1^2)u_1^4+(-2s_1^4+63t_1s_1^3+133t_1^2s_1^2+63t_1^3s_1-2t_1^4)u_1^2\\
&+s_1t_1(23s_1^4-77t_1s_1^3+52t_1^2s_1^2-77t_1^3s_1+23t_1^4))M^{12}+((16s_1^2+99t_1s_1\\
&+16t_1^2)u_1^6-2(6s_1^4+59t_1s_1^3-305t_1^2s_1^2+59t_1^3s_1+6t_1^4)u_1^4+s_1t_1(171s_1^4\\
&-476t_1s_1^3+220t_1^2s_1^2-476t_1^3s_1+171t_1^4)u_1^2+2s_1^2t_1^2(2s_1^4+7t_1s_1^3-10t_1^2s_1^2\\
&+7t_1^3s_1+2t_1^4))M^{10}+u_1((4s_1^2+69t_1s_1+4t_1^2)u_1^6-(12s_1^4+154t_1s_1^3\\
&-355t_1^2s_1^2+154t_1^3s_1+12t_1^4)u_1^4+s_1t_1(227s_1^4-612t_1s_1^3+295t_1^2s_1^2\\
&-612t_1^3s_1+227t_1^4)u_1^2-s_1t_1(18s_1^6+19t_1s_1^5+19t_1^2s_1^4-60t_1^3s_1^3+19t_1^4s_1^2\\
&+19t_1^5s_1+18t_1^6))M^8+(21s_1t_1u_1^8-(4s_1^4+52t_1s_1^3-53t_1^2s_1^2+52t_1^3s_1\\
&+4t_1^4)u_1^6+s_1t_1(125s_1^4-374t_1s_1^3+219t_1^2s_1^2-374t_1^3s_1+125t_1^4)u_1^4+s_1t_1\\
&\times(-30s_1^6-13t_1s_1^5+39t_1^2s_1^4+83t_1^3s_1^3+39t_1^4s_1^2-13t_1^5s_1-30t_1^6)u_1^2-s_1^3\\
&\times(s_1-t_1)^2t_1^3(2s_1+t_1)(s_1+2t_1))M^6+s_1t_1u_1(3u_1^8-(2s_1^2+17t_1s_1+2t_1^2)\\
&\times u_1^6+(23s_1^4-100t_1s_1^3+81t_1^2s_1^2-100t_1^3s_1+23t_1^4)u_1^4+(-12s_1^6+17t_1s_1^5\\
&+80t_1^2s_1^4+11t_1^3s_1^3+80t_1^4s_1^2+17t_1^5s_1-12t_1^6)u_1^2+3s_1^2(s_1-t_1)^2t_1^2(3s_1^2+7t_1s_1\\
&+3t_1^2))M^4+s_1^2t_1^2u_1^2(-9u_1^6+(-4s_1^2+13t_1s_1-4t_1^2)u_1^4+(7s_1^4+23t_1s_1^3\\
&-13t_1^2s_1^2+23t_1^3s_1+7t_1^4)u_1^2+3s_1^2(s_1-t_1)^2t_1^2)M^2+s_1^3t_1^3(s_1^2+t_1s_1+t_1^2)u_1^3((s_1-t_1)^2+3u_1^2)\}
\end{aligned}
\tag{A8}
$$

APPENDIX B: KINEMATICS

We consider the frame in which the proton and electron are moving along $-z$ and $+z$-axes, respectively, and their four momenta are given by

$$P = \frac{\sqrt{s}}{2}(1,0,0,-1), \qquad l = \frac{\sqrt{s}}{2}(1,0,0,1). \tag{B1}$$

The C.M energy of electron-proton system is $s = (P+l)^2$. The above four momenta in light-cone coordinate system can be written as

$$P^\mu = \sqrt{\frac{s}{2}} n_-^\mu, \qquad l^\mu = \sqrt{\frac{s}{2}} n_+^\mu, \tag{B2}$$

where n_+ and n_- are two light-like vectors with $n_+.n_- = 1$ and $n_+^2 = n_-^2 = 0$.

$$n_+^\mu = (1,0,\mathbf{0}), \qquad n_-^\mu = (0,1,\mathbf{0}). \tag{B3}$$

We assume that the quasireal photon is collinear to the electron. The quasi-real photon and gluon four momenta are given by

$$q^\mu = x_\gamma \sqrt{\frac{s}{2}} n_+^\mu, \tag{B4}$$

$$k = \frac{k_{\perp g}^2}{2x_g\sqrt{\frac{s}{2}}} n_+^\mu + x_g\sqrt{\frac{s}{2}} n_-^\mu + \boldsymbol{k}_\perp^\mu \approx x_g\sqrt{\frac{s}{2}} n_-^\mu + \boldsymbol{k}_\perp^\mu, \tag{B5}$$

where $x_\gamma = \frac{q^+}{l^+}$ and $x_g = \frac{k^-}{P^-}$ are the light-cone momentum fractions. The four momentum of the J/ψ is given by

$$P_h^\mu = z x_\gamma \sqrt{\frac{s}{2}} n_+^\mu + \frac{M^2 + P_T^2}{2 z x_\gamma \sqrt{\frac{s}{2}}} n_-^\mu + \boldsymbol{P}_T^\mu. \tag{B6}$$

The inelastic variable is defined as $z = \frac{P.P_h}{P.q} = \frac{P_h^+}{q^+}$. By using the above relations, we can write down the expressions of Mandelstam variables as below

$$\hat{s} = (k+q)^2 = 2k.q = s x_g x_\gamma, \tag{B7}$$

$$\begin{aligned}\hat{t} &= (k - P_h)^2 = M^2 - 2k.P_h \\ &= M^2 - z s x_g x_\gamma + 2k_{\perp g} P_T \cos(\phi - \phi_h),\end{aligned} \tag{B8}$$

$$\hat{u} = (q - P_h)^2 = M^2 - 2q.P_h = M^2 - \frac{M^2 + P_T^2}{z}. \tag{B9}$$

Here M being the mass of J/ψ. The ϕ and ϕ_h are the azimuthal angles of the gluon and J/ψ transverse momentum vector respectively. $\phi_h = 0$ for estimating the asymmetry since the production of J/ψ is considered to be in the xz plane as shown in Fig. 1. The delta function in Eq. (2) can be used to find the solution of x_g. From Eq. (B7)–(B9), the delta function can be written as follows

$$\begin{aligned}&\delta(\hat{s} + \hat{t} + \hat{u} - M^2) \\ &= \delta\Big(s x_g x_\gamma + M^2 - z s x_g x_\gamma + 2k_{\perp g} P_T \cos(\phi - \phi_h) \\ &\quad + M^2 - \frac{M^2 + P_T^2}{z} - M^2 \Big) \\ &= \delta\Big(s x_g x_\gamma (1-z) + 2k_{\perp g} P_T \cos(\phi - \phi_h) - \frac{M^2 + P_T^2}{z} + M^2 \Big) \\ &= \frac{1}{s x_\gamma (1-z)} \delta(x_g - a_1),\end{aligned} \tag{B10}$$

where a_1 is defined as

$$a_1 = \frac{M^2 + P_T^2 - z M^2 - 2z k_{\perp g} P_T \cos(\phi - \phi_h)}{s x_\gamma z (1-z)}. \tag{B11}$$

The phase space integration of J/ψ can be written as

$$\frac{d^3 \boldsymbol{P}_h}{E_h} = \frac{1}{z} dz d^2 \boldsymbol{P}_T. \tag{B12}$$

In line with Ref. [30], we impose the following kinematical cuts on Mandelstam variables

$$M^2 \le \hat{s} \le s, \quad 0 \ge \hat{t} \ge -(\hat{s} - M^2), \quad 0 \ge \hat{u} \ge -(\hat{s} - M^2). \tag{B13}$$

[1] D. W. Sivers, Phys. Rev. D **41**, 83 (1990).
[2] D. W. Sivers, Phys. Rev. D **43**, 261 (1991).
[3] A. Airapetian *et al.* (HERMES Collaboration), Phys. Rev. Lett. **94**, 012002 (2005).
[4] A. Airapetian *et al.* (HERMES Collaboration), Phys. Rev. Lett. **103**, 152002 (2009).
[5] A. Airapetian *et al.* (HERMES Collaboration), Phys. Lett. B **728**, 183 (2014).
[6] C. Adolph *et al.* (COMPASS Collaboration), Phys. Lett. B **717**, 383 (2012).
[7] C. Adolph *et al.* (COMPASS Collaboration), Phys. Lett. B **736**, 124 (2014).

[8] C. Adolph *et al.* (COMPASS Collaboration), Phys. Lett. B **772**, 854 (2017).
[9] M. Aghasyan *et al.* (COMPASS Collaboration), Phys. Rev. Lett. **119**, 112002 (2017).
[10] X. Qian *et al.* (Jefferson Lab Hall A Collaboration), Phys. Rev. Lett. **107**, 072003 (2011).
[11] Y. X. Zhao *et al.* (Jefferson Lab Hall A Collaboration), Phys. Rev. C **90**, 055201 (2014).
[12] A. Adare *et al.* (PHENIX Collaboration), Phys. Rev. D **82**, 112008 (2010); **86**, 099904(E) (2012).
[13] L. Adamczyk *et al.* (STAR Collaboration), Phys. Rev. Lett. **116**, 132301 (2016).
[14] J. C. Collins, Phys. Lett. B **536**, 43 (2002).
[15] D. Boer, P. J. Mulders, and F. Pijlman, Nucl. Phys. **B667**, 201 (2003).
[16] M. Anselmino, M. Boglione, U. D'Alesio, F. Murgia, and A. Prokudin, J. High Energy Phys. 04 (2017) 046.
[17] P. J. Mulders and J. Rodrigues, Phys. Rev. D **63**, 094021 (2001).
[18] M. G. A. Buffing, A. Mukherjee, and P. J. Mulders, Phys. Rev. D **88**, 054027 (2013).
[19] R. M. Godbole, A. Misra, A. Mukherjee, and V. S. Rawoot, Phys. Rev. D **85**, 094013 (2012).
[20] A. Mukherjee and S. Rajesh, Eur. Phys. J. C **77**, 854 (2017).
[21] D. Boer, Few Body Syst. **58**, 32 (2017).
[22] M. Anselmino, V. Barone, and M. Boglione, Phys. Lett. B **770**, 302 (2017).
[23] D. Boer, P. J. Mulders, C. Pisano, and J. Zhou, J. High Energy Phys. 08 (2016) 001.
[24] M. Anselmino, M. Boglione, U. D'Alesio, E. Leader, and F. Murgia, Phys. Rev. D **70**, 074025 (2004).
[25] U. D'Alesio, F. Murgia, C. Pisano, and P. Taels, Phys. Rev. D **96**, 036011 (2017).
[26] A. Mukherjee and S. Rajesh, Phys. Rev. D **93**, 054018 (2016).
[27] A. Mukherjee and S. Rajesh, Phys. Rev. D **95**, 034039 (2017).
[28] G. T. Bodwin, E. Braaten, and G. P. Lepage, Phys. Rev. D **51**, 1125 (1995); **55**, 5853(E) (1997).
[29] C. E. Carlson and R. Suaya, Phys. Rev. D **14**, 3115 (1976).
[30] E. L. Berger and D. L. Jones, Phys. Rev. D **23**, 1521 (1981).
[31] R. Baier and R. Ruckl, Phys. Lett. B **102B**, 364 (1981).
[32] R. Baier and R. Ruckl, Nucl. Phys. **B201**, 1 (1982).
[33] E. Braaten and S. Fleming, Phys. Rev. Lett. **74**, 3327 (1995).
[34] P. L. Cho and A. K. Leibovich, Phys. Rev. D **53**, 150 (1996).
[35] P. L. Cho and A. K. Leibovich, Phys. Rev. D **53**, 6203 (1996).
[36] G. P. Lepage, L. Magnea, C. Nakhleh, U. Magnea, and K. Hornbostel, Phys. Rev. D **46**, 4052 (1992).
[37] F. Abe *et al.* (CDF Collaboration), Phys. Rev. Lett. **79**, 572 (1997).
[38] D. Acosta *et al.* (CDF Collaboration), Phys. Rev. D **71**, 032001 (2005).
[39] C. Adloff *et al.* (H1 Collaboration), Eur. Phys. J. C **25**, 25 (2002).
[40] F. D. Aaron *et al.* (H1 Collaboration), Eur. Phys. J. C **68**, 401 (2010).
[41] S. Chekanov *et al.* (ZEUS Collaboration), Eur. Phys. J. C **27**, 173 (2003).
[42] H. Abramowicz *et al.* (ZEUS Collaboration), J. High Energy Phys. 02 (2013) 071.
[43] M. Butenschoen and B. A. Kniehl, Phys. Rev. Lett. **106**, 022003 (2011).
[44] Y.-Q. Ma, K. Wang, and K.-T. Chao, Phys. Rev. D **84**, 114001 (2011).
[45] K.-T. Chao, Y.-Q. Ma, H.-S. Shao, K. Wang, and Y.-J. Zhang, Phys. Rev. Lett. **108**, 242004 (2012).
[46] M. Butenschoen and B. A. Kniehl, Phys. Rev. D **84**, 051501 (2011).
[47] H.-F. Zhang, Z. Sun, W.-L. Sang, and R. Li, Phys. Rev. Lett. **114**, 092006 (2015).
[48] M. Butenschoen and B. A. Kniehl, Phys. Rev. Lett. **108**, 172002 (2012).
[49] F. Yuan, Phys. Rev. D **78**, 014024 (2008).
[50] J. Matouek (COMPASS Collaboration), J. Phys. Conf. Ser. **678**, 012050 (2016).
[51] B. A. Kniehl and G. Kramer, Eur. Phys. J. C **6**, 493 (1999).
[52] M. G. Ryskin, Z. Phys. C **57**, 89 (1993).
[53] M. Butenschoen and B. A. Kniehl, Phys. Rev. Lett. **104**, 072001 (2010).
[54] Y.-d. Li and L.-s. Liu, Commun. Theor. Phys. **29**, 99 (1998).
[55] P. Artoisenet, J. M. Campbell, F. Maltoni, and F. Tramontano, Phys. Rev. Lett. **102**, 142001 (2009).
[56] M. Kramer, Nucl. Phys. **B459**, 3 (1996).
[57] P. Ko, J. Lee, and H. S. Song, Phys. Rev. D **54**, 4312 (1996); **60**, 119902(E) (1999).
[58] U. D'Alesio, C. Flore, and F. Murgia, Phys. Rev. D **95**, 094002 (2017).
[59] S. Frixione, M. L. Mangano, P. Nason, and G. Ridolfi, Phys. Lett. B **319**, 339 (1993).
[60] U. D'Alesio, F. Murgia, and C. Pisano, J. High Energy Phys. 09 (2015) 119.
[61] A. Adare *et al.* (PHENIX Collaboration), Phys. Rev. D **90**, 012006 (2014).
[62] D. Boer and W. Vogelsang, Phys. Rev. D **69**, 094025 (2004).
[63] R. Baier and R. Ruckl, Z. Phys. C **19**, 251 (1983).
[64] D. Boer and C. Pisano, Phys. Rev. D **86**, 094007 (2012).
[65] J. H. Kuhn, J. Kaplan, and E. G. O. Safiani, Nucl. Phys. **B157**, 125 (1979).
[66] B. Guberina, J. H. Kuhn, R. D. Peccei, and R. Ruckl, Nucl. Phys. **B174**, 317 (1980).
[67] A. D. Martin, W. J. Stirling, R. S. Thorne, and G. Watt, Eur. Phys. J. C **63**, 189 (2009).
[68] J. Kuipers, T. Ueda, J. A. M. Vermaseren, and J. Vollinga, Comput. Phys. Commun. **184**, 1453 (2013).
[69] M. Anselmino, M. Boglione, U. D'Alesio, S. Melis, F. Murgia, and A. Prokudin, Phys. Rev. D **81**, 034007 (2010).